Final Report
for the project

Advanced Photonic Materials Produced By Containerless Processing
(12/01/91 to 02/29/96)
Contract NAGW-2846

Prepared for

National Aeronautics and Space Administration

Prepared by

Chandra S. Ray and Delbert E. Day
Ceramic Engineering Department and
Graduate Center for Materials Research
University of Missouri-Rolla
Rolla, MO 65409-1170.

Phone: (573)341-4354
Fax: (573)341-2071
E-mail: day@umr.edu

30 November, 1996

U M
r

UNIVERSITY OF MISSOURI-ROLLA
Missouri's Technological University

30 November, 1996

Dr. Robert C. Rhome
Microgravity Science and application Division
National Aeronautics and Space Administration
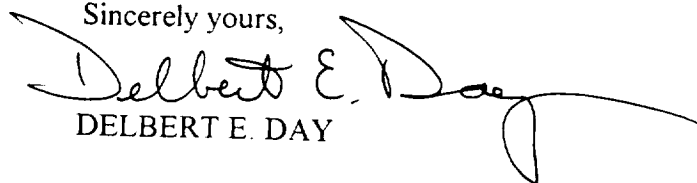UGS (940345)
Washington, DC 20546-0001.

Dear Dr. Rhome:

Enclosed is the final report for our project "Advanced Photonic Materials Produced by Containerless Processing", NASA contract NAGW-2846, from 12/01/91 to 02/29/96. As can be seen from the report, this has been a highly productive project which yielded several outstanding and very useful results. Some of the major achievements accomplished in this research are as follows.

1. A pure TeO_2 glass of usuable quantity was prepared for the first time.
2. A new class of optical glasses based on PbO, Nb_2O_5, and TeO_2 was developed, which are shown to have a high nonlinear refractive index and are believed to be promising candidates for use as high speed optical switches and shutters.
3. A DTA technique that distinguishes internal from surface crystallization was developed. This DTA technique is much faster than the traditional experimental method of determining the crystallization mechanism and has proved to be universally applicable to most inorganic oxide glasses.
4. An active and productive collaboration with Japanese Space Program has been established through Osaka National Research Institute (ONRI) in Japan. Glass melting experiments in low gravity are continuing using the world's longest drop shaft (710 m) at Japan Microgravity Center (JAMIC) in collaboration between University of Missouri-Rolla and ONRI --- all at Japanese Government expense.
5. This research has culminated in 10 presentations in national and international meetings and 21 publications in leading technical journals.

I am confident that the goals of the research project have been met and the work described in this report is of high standard. The researchers involved in this project, particularly, Chandra Ray and myself, wish to express our thanks to you and your colleagues for funding this research. If you have any question regarding the technical content of this report, please feel free to contact me.

Sincerely yours,

DELBERT E. DAY

cc to:
Drs. A. Biswas and Angela Belcastro, JPL

Final Report
for the project

Advanced Photonic Materials Produced By Containerless Processing
(12/01/91 to 02/29/96)
Contract NAGW-2846

Prepared for

National Aeronautics and Space Administration

Prepared by

Chandra S. Ray and Delbert E. Day
Ceramic Engineering Department and
Graduate Center for Materials Research
University of Missouri-Rolla
Rolla, MO 65409-1170.

Phone: (573)341-4354
Fax: (573)341-2071
E-mail: day@umr.edu

30 November, 1996

Table of Contents

1. Introduction:

There is a major and growing interest in developing photonic or all-optical switching and signal processing devices for future communications and computing applications [1-3]. All-optical switching and routing devices which use the non-linear optical (NLO) properties (e.g., the non-linear refractive index) of a material, have the advantage of operating at speeds and band widths much greater than those of electronic devices. Optical glasses are considered promising candidates for such devices because they can be made to possess a rapid non-linear response to an optical signal, a high damage threshold, optical transparency over a large wavelength range, and physical, chemical and thermal properties that are suitable for practical applications.

It has been found that glasses with a high density and linear refractive index along with a low dispersion usually have a high non-linear refractive index. The heavy metal oxide (HMO) glasses containing PbO, Bi_2O_3, and Ga_2O_3 are reported[2,4] to have a high density (>8 g/cm^3) and refractive index (>2), and excellent NLO properties. However, these HMO glasses develop a strong color (yellow to brown) and tend to crystallize during cooling, so these glasses are unsuitable for NLO applications.

Their color is reported[2] to be caused by materials dissolved from the container during melting. The tendency for these melts to react with all known containers and to crystallize, makes them excellent candidates for containerless processing. Also, the physical, chemical, and thermal properties, which need to be known for a material to determine its suitability for practical application, are not well documented for these HMO glasses.

The present research deals with the glass formation characteristics and properties of compositions containing PbO, Bi_2O_3, and Ga_2O_3. The properties that have been investigated as a function of composition include density, molar volume, thermal expansion coefficient, chemical durability, glass transition temperature, crystallization temperature, and transmission in the ultraviolet-visible (UV-visible) and IR.

Attempts were made to obtain colorless glasses in the PbO-Bi_2O_3-Ga_2O_3 system either by changing the parameters that generally affect the color of a glass such as the melting temperature, time, and atmosphere, crucible material and the starting raw materials or by processing the glass without using a container (containerless melting). As it will be discussed later, no suitable conditions were found which totally eliminated the color and yielded totally colorless glasses.

3

Since the color of the PbO-Bi$_2$O$_3$-Ga$_2$O$_3$ glasses could not be totally eliminated even by containerless melting, the present investigation was extended to other HMO glasses having potential use in NLO applications. One such class of glasses are those containing tellurium oxide. Although tellurium oxide (TeO$_2$) itself is not a traditional glass former, it forms a glass when combined with many other inorganic oxides[5-7]. Since glasses with a high density and linear refractive index have, generally, a high nonlinear refractive index, compositions in the systems PbO-TeO$_2$, Bi$_2$O$_3$-TeO$_2$, and PbO-Bi$_2$O$_3$-TeO$_2$ were investigated initially. The addition of PbO and Bi$_2$O$_3$ was expected to increase the density and refractive index of the telluride glasses. The purpose was to develop a tellurite glass suitable for nonlinear optical applications, especially for all-optical switches or shutters. Unfortunately, the glass forming region in all these systems was too small for practical use, being smallest for Bi$_2$O$_3$ compositions.

Glass formation was found to improve when Nb$_2$O$_5$ was added to compositions containing PbO and TeO$_2$ and a new class of glasses in the PbO-Nb$_2$O$_5$-TeO$_2$ (PNT) ternary system were prepared for the first time. The reason for selecting Nb$_2$O$_5$ as the third component arose from the fact that crystals containing Nb$_2$O$_5$, such as the lithium niobate have excellent NLO properties, and the origin of optical nonlinearity in these crystals is attributed[3,8] to the Nb^{5+} ions. PbO-Nb$_2$O$_5$-TeO$_2$ glasses were, therefore, anticipated to have excellent NLO properties. In addition, glass formation and properties of pure TeO$_2$ and Na$_2$O-TeO$_2$ glasses were investigated in order to gain a better understanding of (1) the kinetics of glass formation for tellurite melts and (2) the structural role of Te-ions in the tellurite glasses.

2. Objectives:

The objectives of this research were as follows.

1. To investigate the mechanism of glass formation using traditional and containerless glass melting techniques for NLO glasses which have the potential for use as ultrafast, all optical switches and other photonic devices for communication and advanced computer application.

2. To measure selected properties which determine the suitability of a glass for practical applications, such as its density, refractive index, thermal expansion coefficient, chemical durability, glass transition

4

and crystallization temperatures, and transmission in the ultraviolet-visible and infrared.

3. To measure the IR and Raman spectra to determine the structure of these glasses.

4. To investigate the kinetics of nucleation and crystallization for selected glasses.

Investigations of the NLO glasses were conducted primarily with two HMO compositional systems: (1) $PbO-Bi_2O_3-Ga_2O_3$ and (2) compositions based on TeO_2, namely, pure TeO_2, Na_2O-TeO_2, and $PbO-Nb_2O_5-TeO_2$.

3. Results and Discussion:
3.1. PbO-Bi₂O₃-Ga₂O₃ Glasses:
3.1.1. Color:

Among all the oxide glasses investigated to-date, the HMO glasses containing PbO, Bi_2O_3, and Ga_2O_3 are reported[2,4] to have the best nonlinear optical properties. However, their orange to yellow color is a potential disadvantage for their use in many applications, especially in optical devices. The initial task of the present work, therefore, was to investigate how the color of $PbO-Bi_2O_3-Ga_2O_3$ glasses could be eliminated.

First, those melting parameters known to affect the color of glasses such as the crucible material, melting temperature, time and atmosphere, and the starting raw materials were changed systematically in an attempt to obtain colorless glasses. The range of compositions investigated was $xPbO.(100-(x+y))BiO_{1.5}.yGaO_{1.5}$, cat%, where x varied from 20 to 60 and y equalled 20, 25, 30, or 35, see also Table 1. The glasses were melted at 850°, 900°, 950°, and 1000°C for 30 or 60 min in either alumina, gold, or platinum crucibles. The furnace atmosphere was either air, nitrogen, or oxygen with a flow rate of about 660 cm^3/min. Part of the lead oxide was replaced by PbF_2, and $Ga(NO_3)_3$ was used in place of Ga_2O_3. Glasses containing small amounts (0.01 to 0.05 wt%) of Cr_2O_3, Co_3O_4, and CeO_2 were also made to investigate their decolorizing effect in these glasses. While the color was greatly reduced, no conditions were found which totally eliminated the color. The least color, pale yellow, was obtained for a $40PbO.35BiO_{1.5}.25GaO_{1.5}$, cat%, glass (HMO-7, Table 2) when it was melted in air or in a nitrogen atmosphere in an alumina or gold crucible at 900°C for 30 min.

5

Since the HMO-7 glass had the least color, it was melted using two different containerless melting techniques developed at UMR in order to investigate whether containerless melting would totally eliminate the color from this glass. In both containerless melting techniques, a presintered batch with particle size between 75 and 150 μm was used as the starting material. In one technique, the sintered powder was fed into a high temperature gas flame, where the batch particles melted while passing through the high temperature flame. The molten particles formed spherical droplets due to surface tension, solidified when in flight, and were collected in a stainless steel drum which surrounded the flame.

In the second technique, the solid (sintered) particles were dropped into the top of a vertical tube furnace. The spherical droplets formed from the melted particles were quenched in cold water at the bottom of the furnace tube. Spherical glass beads 60 to 200 μm in diameter were easily obtained in both containerless melting techniques. The containerless melted glass beads, however, also had a pale yellow color, which suggests that the weak yellow color is intrinsic to these glasses.

3.1.2. Properties:

Because of the potential applications of the $PbO-Bi_2O_3-Ga_2O_3$ glasses, knowledge of their properties is of considerable value. Properties such as the density (d), molar volume (V_m), thermal expansion coefficient (α), chemical durability (DR) in solutions of different pH, glass transition (T_g) and crystallization (T_c) temperatures, and transmission in the ultraviolet-visible and IR have been measured as a function of composition and are shown in Table 1. *The methods used to measure these properties and the property values have also been discussed in detail in a technical paper published in the Journal of the American Ceramic Society, Vol. 77, pp. 1017-24 (1994) which is enclosed with this report as Appendix 1.* The investigations on the color of these glasses and the techniques, including containerless melting techniques, used in an attempt to decolorize these glasses are also described in this paper.

The results for the properties of these HMO glasses are briefly summarized below. The density, d, for these glasses decreases slowly as PbO replaces $BiO_{1.5}$ for a constant $GaO_{1.5}$ content. Replacing either $BiO_{1.5}$ (constant PbO) or PbO (constant $BiO_{1.5}$) by $GaO_{1.5}$ causes a more rapid decrease in density. V_m decreases slowly when $GaO_{1.5}$ replaces $BiO_{1.5}$ for a constant PbO content, but decreases at a faster rate when PbO replaces $BiO_{1.5}$ for a constant $GaO_{1.5}$ content.

6

Replacing PbO by $GaO_{1.5}$ at constant $BiO_{1.5}$ causes V_m to increase. The compositional dependence of d and V_m for these glasses correlate with the weight and size of Pb^{2+}, Bi^{3+}, Ga^{3+}, and O^{2-} ions in each glass.

The average value of the thermal expansion coefficient, α, decreases and T_g increases as $GaO_{1.5}$ replaces either PbO or $BiO_{1.5}$ which is consistent with the charge and bond strength of the cations in these HMO glasses, see Appendix 1. It appears that the network structure becomes stronger with increasing $GaO_{1.5}$, suggesting that Ga^{3+} ions act as network formers. No significant change in α and T_g occurs when PbO replaces $BiO_{1.5}$, which indicates that the lead and bismuth ions have, generally, the same role in these HMO glasses. The observed compositional dependence of α and T_g when PbO replaces $BiO_{1.5}$ cannot be fully explained if all the lead ions are present as Pb^{2+} in these glasses, but can be explained satisfactorily if about 30 to 40% of the lead ions are assumed to be present as Pb^{4+}.

The dissolution rate, DR, for these glasses in deionized water (pH 6.9), HCl (pH 4.0), and in NaOH (pH 10.0) at 25°C is nearly independent of the solution pH, but depends strongly on the lead content. The DR increases by about 4 orders of magnitude (from ~ 10^{-8} to 10^{-4}) as the PbO content increases from 20 to 60 cat% and remains constant as PbO replaces either $GaO_{1.5}$ or $BiO_{1.5}$. All of the dissolution rate results are consistent with the bond strength of the cations. Since the bond strength of the lead ions (especially that of Pb^{2+}) is the lowest among the three cations, lead is the least tightly bonded component in the glass and is leached from these glasses when immersed in water, HCl, or NaOH.

The crystallization temperature, T_c, for these HMO glasses increases as $GaO_{1.5}$ replaces either PbO or $BiO_{1.5}$. The difference $(T_c - T_g)$ which is frequently used as a measure of the glass formation tendency, also increases as $GaO_{1.5}$ replaces either PbO or $BiO_{1.5}$. No significant change in $(T_c - T_g)$ occurs when PbO replaces $BiO_{1.5}$. These results suggest that Ga_2O_3 improves glass formation and suppresses crystallization in these HMO glasses. The role of PbO anf $BiO_{1.5}$ is almost the same in these glasses and, in general, reduces the tendency for glass formation.

These HMO glasses have a high absorption edge (cut off wave length), about 8 μm, in the infrared which remain nearly unchanged for the glasses studied in the present investigation. The UV-visible absorption edge shifts toward longer wavelengths, from about 470 to 498 nm, as either PbO or $BiO_{1.5}$ replaces $GaO_{1.5}$. Also, for a constant $GaO_{1.5}$ content, the absorption edge shifts slowly toward the

7

longer wavelengths as PbO replaces $BiO_{1.5}$. These results suggest that the intrinsic yellow color of these glasses is due to the combined presence of lead and bismuth ions and that the lead ions have a stronger effect in producing color.

3.1.3. Crystallization:

The crystallization of these HMO glasses was investigated using differential thermal analysis (DTA) and high temperature x-ray diffraction analysis (XRD). The typical crystallization exotherm present in the DTA curves for a few selected glasses is shown in Fig. 1. These DTA curves were obtained at a heating rate of 10°C/min and using glass particles <38 μm. The crystallization temperature as well as the number of crystallization peaks clearly change with composition. For the high lead glasses (curves #12 and 14 in Fig. 1, HMO-12 and 14 in Table 2), primarily one crystallization peak is present in the DTA curve, while for the low lead glasses (curves #1 and 5, HMO-1 and 5 in Table 2), more than one crystallization peak is usually present.

To identify the crystals responsible for the DTA peaks, the glass samples crystallized in DTA were analyzed by XRD. Two separate XRD measurements were made for each glass. In the first case, the DTA furnace was turned off immediately after the first crystallization peak was complete, the temperature ranged from 390 to 460°C for different glasses in this case. In the second case, the DTA measurements continued until crystallization was totally complete (~ 550°C). The XRD patterns for the samples in the first case (XRD-1) contained only lead oxide, but the exact phase of lead oxide could not be identified definitely in all the patterns. For most of the samples, all possible phases of lead oxide, PbO_x ($1 \leq x \leq 2$), appeared to be present with PbO as the major phase.

No lead oxide was detected in the XRD patterns for the samples in the second case (XRD-2), but all possible lead-bismuth compounds such as $2PbO.3Bi_2O_3$, $5PbO.4Bi_2O_3$, and $2PbO_2.12BiO_3$ might be present. The major phase identified in the XRD-2 patterns was $2PbO_2.12Bi_2O_3$. For high lead containing glasses, which had a single crystallization peak, both XRD patterns (XRD-1 and XRD-2) contained only PbO. A list of compounds detected in these two XRD patterns for the glasses crystallized in DTA is given in Table 2.

To understand more about the crystallization of these glasses, XRD patterns were obtained at 420, 480, 500, and 575°C, see Fig. 2, for a $20PbO-60BiO_{1.5}$-$20GaO_{1.5}$, cat%, glass (HMO-1, Table 2), which is typical of the glasses that show multiple exothermic peaks during crystallization in DTA (Fig. 1). These

8

temperatures were chosen from the temperature range where DTA peaks were located for this glass. The sample was held at each temperature for 30 min before the high temperature XRD measurements were made. The XRD pattern for the as-quenched glass is also included in Fig. 2 for comparison.

In the XRD pattern at 420°C, PbO is the only crystalline phase present. At 480°C, two crystalline phases are present, primarily $2PbO.3Bi_2O_3$ and a small amount of $2PbO_2.12Bi_2O_3$. At 500 and 575°C, the major crystalline compound identified by XRD is $2PbO_2.12Bi_2O_3$, while $2PbO.3Bi_2O_3$ is a minor phase. Comparison of Figs. 1 and 2 indicates that PbO crystallizes first from this glass at a relatively low temperature (between 390 and 425°C), and then reacts with the remaining glass with increasing temperature to form the lead-bismuth compounds, namely, $2PbO.3Bi_2O_3$ at ~460 to 490°C and $2PbO_2.12Bi_2O_3$ above 500°C. Unlike the XRD results for samples crystallized in DTA (for example HMO-1, Table 2), no form of lead oxide other than PbO or the compound $5PbO.4Bi_2O_3$ were detected in the high temperature XRD measurements. These results suggest that the other forms of lead oxide (than PbO) and the $5PbO.4Bi_2O_3$ compound are not sufficiently stable.

It is interesting to note that the high temperature (above 500°C) crystallization product, $2PbO_2.12Bi_2O_3$, of the HMO-1 glass (Table 2) contains PbO_2 as opposed to PbO which was in the crystals $2PbO.3Bi_2O_3$ formed at temperatures below 500°C. This means that an oxidation process (PbO → PbO_2) takes place in this glass at and above 500°C. The additional oxygen, probably, comes from the surrounding air. To verify this result, thermogravimetric analysis (TGA) was performed in air, oxygen, and nitrogen for the HMO-1 glass, see Fig. 3. An increase in weight (oxidation) is clearly observed above 500°C in the TGA curves measured in air or oxygen, but there is no weight increase when the TGA is performed in an oxygen-free atmosphere such as nitrogen.

3.1.4. Nucleation and Crystallization Kinetics:

Except for the glasses containing a high amount of PbO (50 to 60, cat%), all the glasses investigated in the $PbO-Bi_2O_3-Ga_2O_3$ system yield multiple DTA crystallization peaks. This makes it difficult to determine either the activation energy for crystallization, E, or the relative nucleation rates at different temperatures (a nucleation rate type curve) for these glasses. A $60PbO.10BiO_{1.5}.30GaO_{1.5}$, cat% (HMO-12) glass, which contains a single DTA crystallization peak, was chosen for determining E. First, the temperature for

9

the DTA crystallization peak maximum, T_p, was determined as a function of heating rate, ϕ, keeping the particle size of the sample constant for all the measurements. The DTA heating rates used were 2, 4, 6, 10, and 15° C/min and the size of the glass particles was between 20 and 38 μm. According to the thermoanalytical model developed by Kissinger[9], T_p and ϕ are related as

$$\ln (T_p^2/\phi) = E/RT_p + \text{constant} \quad \ldots \quad \ldots \quad \ldots \quad (1)$$

where, R is the gas constant. A plot of $\ln(T_p^2/\phi)$ vs $1/T_p$ (Kissinger plot) should be a straight line whose slope contains the activation energy for crystallization, E. The Kissinger plot for the HMO-12 glass in Fig. 4 is a very good straight line and yields a value of E of about 470 $\pm$ 10 kJ/mol. This value of E for the HMO-12 glass is considered high compared to the 300 and 370 kJ/mol values for the more common silicate glasses such as $Li_2O.2SiO_2$[10] and $Na_2O.2CaO.3SiO_2$[11], respectively. A high value of E, generally, ensures, a good glass forming tendency of the melt.

The same HMO-12 glass was used to determine a nucleation rate type curve using the DTA technique developed by ourselves[12]. In this technique, glass samples of constant weight and particle size are first heated isothermally (at T_n) in the DTA furnace for a fixed time (nucleation), and then heated at a constant rate until the glass crystallizes (crystallization). A plot of either the maximum height of the DTA crystallization peak, $(\delta T)_p$, or $1/T_p$ as a function of nucleation temperature, T_n, yields a curve similar to the well known nucleation rate vs temperature curve found in many silicate glasses. It was also demonstrated that the dependence of $(\delta T)_p$ on T_n was more sensitive than that of $1/T_p$ on T_n.

The plots of $(\delta T)_p$ and $1/T_p$ as a function of T_n for the HMO-12 glass are shown in Figs. 5 and 6, respectively. The experimental conditions for these measurements are given in the figure captions. Fig. 5 shows that $(\delta T)_p$ for this glass does not change from that of the as-quenched glass until the glass is nucleated above ~265°C, reaches a maxima at ~343°C, and then decreases to the value for the as-quenched glass at ~375°C. In other words, the temperature for nucleating this glass ranges from ~265° to 375°C and the temperature where the nucleation rate is a maximum, is ~343°C.

No information on the temperature range for nucleation or the temperature for maximum nucleation rate for this glass is obtained from the plot of T_p vs T_n, see Fig. 6. In fact, T_p for a majority of the glass samples nucleated at different

temperatures lies within the $\pm 1.5°C$ limit of experimental error (vertical distance between the pair of broken lines shown in Fig. 6). Instead of yielding a bell-shaped curve, T_p shows an increasing trend, although slightly, with increasing T_n, from ~456°C for the as-quenched glass to ~464°C for the glass nucleated at 395°C for 3 h. The T_p for this HMO-12 glass measured after different nucleation treatment is, therefore, considered random and independent of the nucleation temperature.

Glasses generally crystallize by either surface or internal (volume) crystallization. Although, both crystallization mechanisms can occur simultaneously and competitively, one mechanism usually dominates over the other in most cases.

The present authors have developed[13] a DTA technique which is fast, convenient, and requires only a small quantity (about 500 mg) of sample, for identifying the dominant crystallization (surface vs internal) mechanism in glasses. In this method, either $(\delta T)_p$ or the ratio $T_p^2/(\Delta T)_p$, where $(\Delta T)_p$ is the peak half width, is measured using DTA and plotted as a function of the glass particle size, keeping the amount of glass sample and the DTA heating rate constant for all the measurements. Both $(\delta T)_p$ and $T_p^2/(\Delta T)_p$ were found to decrease with increasing particle size when surface crystallization is the dominant mechanism and to increase (with increasing particle size) when internal crystallization becomes predominant.

The values of $(\delta T)_p$ and $T_p^2/(\Delta T)_p$ for the HMO-12 glass have been measured at a constant DTA heating rate of 15° C/min for a sample weighing 40 ± 0.5 mg. The results are plotted as a function of particle size in Fig. 7. Both $(\delta T)_p$ and $T_p^2/(\Delta T)_p$ for this glass decrease with increasing particle size indicating that this HMO-12 glass crystallizes primarily by surface crystallization.

3.1.5. IR and Raman Spectra:

To evaluate the structure of these $PbO-Bi_2O_3-Ga_2O_3$ glasses, the IR and Raman spectra of the glasses and their devitrified counterparts were measured as a function of composition. The IR spectra were measured from 400 to 3500 cm^{-1} using the standard KBr pellet technique and the Raman spectra were measured from 10 to 1500 cm^{-1} using 514.5 μm light from a 50 mW argon ion laser. Results from both IR and Raman spectra suggest that most of the Ga^{3+} ions exist in GaO_4 groups and act primarily as network forming cations in these glasses. A part of the Ga^{3+} ions appear to be in 6-fold coordination (GaO_6 group) when the

11

Ga^{3+} content exceeds about 30%. Pb^{2+} and Bi^{3+} ions act primarily as network modifying cations forming tetragonal PbO$_4$ (and/or trigonal PbO$_3$) groups and distorted BiO$_6$ octahedra, respectively. In high lead or bismuth containing glasses (>50 cat%), some of the Pb^{2+} and Bi^{3+} ions are believed to act as network forming cations. The structural information obtained from the IR and Raman spectra of these HMO glasses are consistent with those predicted from their observed physical, thermal, and chemical properties, see section A2 above and also Appendix 1. *The results of Raman spectra for the PbO-Bi$_2$O$_3$-Ga$_2$O$_3$ glasses are described in a technical paper that has been accepted for publication in the Physics and Chemistry of Glasses. A preprint of that paper is enclosed in Appendix 2.*

3.2. Tellurium Oxide (TeO$_2$) Glass:

Although tellurium dioxide readily forms glass when combined with many other inorganic oxides, TeO$_2$ itself is not a traditional glass former. Attempts to prepare a glass by quenching a melt of TeO$_2$ have been unsuccessful up to this time due to rapid crystallization of the melt. Using a rapid quenching technique (by dipping the bottom of a crucible holding the TeO$_2$ melt in ice water), only a small amount (200 mg maximum at each attempt) of TeO$_2$ glass has been prepared[3]. Thus, information on the formation and properties of pure TeO$_2$ glass is quite limited at this time.

A flame-spraying technique described elsewhere[14,15] and shown schematically in Fig. 8 was used to prepare glass beads of pure TeO$_2$ composition in the present investigation. Commercially available crystalline TeO$_2$ powders (99.99% pure) were passed through a propane-oxygen flame which was positioned at one end of a stainless steel cylindrical drum. The crystalline TeO$_2$ particles melt while passing through the flame (TeO$_2$ melts at 732° C), the molten droplets become spherical due to surface tension and then solidify before being collected at the bottom of the drum. The glass beads so prepared are annealed at about 230° C and washed with acetone.

An example of the glass beads made by this process from pure TeO$_2$ is shown in Fig. 9A. These beads vary in diameter from 40 to 75 μm. When these beads were analyzed by energy dispersive x-ray analysis (EDAX), no elements other than Te was detected (oxygen cannot be detected by EDAX). Although this TeO$_2$ glass was obtained in the form of small beads, this process can be automated for large scale production, several kg/hour, depending upon the size of the gas

12

burner.

A white layer was found on the inside, top surface of the cylindrical drum (Fig. 8), which is believed to have formed from the vapor of TeO_2 melt. When analyzed by scanning electron microscopy (SEM), this white layer was found to contain glass spheres of much smaller diameter (<1 μm, Fig. 9B) than that of the spheres collected at the bottom of the drum (Fig. 9A). EDAX analysis of these beads showed that they contained only Te. A similar white layer, which was composed of TeO_2 glass spheres ranging from 1 to 10 μm in diameter, was formed when a $Na_2O.4TeO_2$ glass was evaporated in the low gravity environment of a drop shaft[16]. This white layer in the low gravity experiment was deposited on the walls of a glass container that was used to trap the species evaporated from the $Na_2O.4TeO_2$ melt, see also section 3.3.3.

3.2.1. X-ray Diffraction Analysis (XRD) and Differential Scanning Calorimetry (DSC):

To differentiate between the two types of beads obtained by flame spraying crystalline TeO_2 powders, the relatively larger beads collected at the lower part of the cylindrical drum will be hereafter referred to as flame sprayed or "FS beads" and those deposited at the upper part of the drum will be referred to as vapor deposited or "VD beads". The XRD patterns of the FS beads and VD beads shown in Fig. 10 clearly demonstrates that both beads were totally glassy. The presence of sharp exothermic crystallization peaks in their DSC thermograms, see Fig. 11, also confirms that both types of beads were totally glassy in their as-made condition and crystallize, most likely, to a single phase.

Both types of beads contain no elements other than Te. However, the crystallization temperature, T_c, (temperature corresponding to the onset of the crystallization peak) for the two types of beads are totally different (Fig. 11). The FS beads crystallize at a much lower temperature ($273 \pm 2°$ C) than the VD beads ($314 \pm 2°$ C). Also, the area of the crystallization peak for the FS beads is about 4 times larger than that of the VD beads for a comparable amount of sample. These DSC results suggest that the composition of the FS beads and VD beads may be significantly different and that the VD beads are more resistant to crystallization than the FS beads.

The activation energy for crystallization, E, for these glass beads was determined by DSC at heating rates of 5, 10, 20, 30 and 40° C/min and employing Kissinger's method of data analysis, see eqn. 1. The Kissinger plots

13

for the two types of glass beads in Fig. 12 yield a value of E of about 172 ± 10 and 418 ± 10 kJ/mol for the FS beads and VD beads, respectively. The much higher value of E for the VD beads supports our previous conclusion that the glass beads prepared by vapor deposition from a tellurium oxide melt are more resistant to crystallization than the glass beads prepared from a melt by flame spraying.

The glass beads were crystallized at temperatures corresponding to the maximum of the DSC crystallization peak, T_p, in Fig. 11 (288° C for the FS beads and 322° C for the VD beads) for 24 h and then analyzed by XRD. As shown in Fig. 13, the peaks in the XRD pattern of the crystallized, flame sprayed glass beads match very well with those of crystalline α-TeO_2 (tetragonal paratellurite), indicating that the composition of the flame sprayed glass beads is TeO_2. The peaks in the XRD pattern of the crystallized, vapor deposited glass beads contain, in addition to the peaks of α-TeO_2, a large number of peaks which have not been identified so that the exact composition of the VD beads remains unknown.

3.2.2. Infrared (IR) and Raman Spectra:

The IR spectra for the FS glass beads, VD glass beads and their crystallized counterparts shown in Fig. 14 were measured by the KBr pellet technique for wavenumbers from 450 to 1500 cm⁻¹. Minor differences in the IR spectra for these samples are clearly evident. The absorption peaks at about 665 cm⁻¹ and 780 cm⁻¹ are more pronounced for the FS glass beads than those for the VD glass beads. Also, for wavenumbers smaller than about 550 cm⁻¹ the spectra for the FS glass beads remain practically constant, whereas, an absorbtion tail is observed in the IR spectra for the VD glass beads. The IR spectra for the crystalline samples of both glass beads are almost identical in the range where the peaks are more pronounced i.e., from 630 cm⁻¹ to 790 cm⁻¹. However, the crystalline sample for the VD beads also contains several small peaks at about 457 cm⁻¹, 487 cm⁻¹, and 546 cm⁻¹, which are not observed in the IR spectra for the crystalline sample of the FS beads. The absorbtion tail in the IR spectra for the VD glass beads at wavenumbers smaller than 550 cm⁻¹ is consistent with the presence of several small absorption peaks in the spectra for the crystalline VD beads below 550 cm⁻¹. The IR spectra for the crystalline FS beads are identical to that of crytalline TeO_2 raw materials (α-TeO_2), see Fig. 15.

Comparison of the IR spectra of the FS glass beads, VD glass beads, their

crystals, and the TeO_2 raw materials indicate that the chemical composition of the glass beads prepared from the melt of TeO_2 by flame spraying is different from that of the glass beads prepared by condensing the vapor of the TeO_2 melt and that the crystals formed from these two types of glass beads are also different. The composition of the glass beads prepared from the melt of TeO_2 by flame spraying is close to TeO_2 and crystalline, tetragonal α-TeO_2 (paratellurite) crystallizes from this glass. These results are consistent with the DSC and XRD resualts for the glass beads and their crystals, see section 3.2.2 above.

The Raman spectra of the glass and crystallized beads, which are shown in Figs. 16 and 17, respectively, were obtained using the 514 nm argon ion line for excitation. No significant difference in the Raman spectra of the FS glass beads and VD glass beads (Fig. 16) or of their crystalline forms (Fig. 17) are observed. Thus, the Raman spectra for these samples does not provide any information for compositional differences between the flame sprayed and vapor deposited glass beads. The broad Raman bands for the glassy beads in Fig. 16 are characteristic of glassy materials. Similar Raman spectra for a TeO_2 glass have been reported[17] by other investigators. The Raman spectra for the crystallized beads in Fig. 17 indicates that both FS beads and VD beads crystallize primarily to tetragonal, paratellurite α-TeO_2 form. The tetragonal, rutile-like form of TeO_2 was also identified as a minor phase. The orthorhombic β-TeO_2 was clearly not present in any of these glassy or crystallized beads.

3.2.3. X-ray Photoelectron Spectra (XPS):

The XPS spectra were recorded using a spectrometer (Physical Electronics, Model #548) with Mg Kα (hv = 1254.6 eV) radiation as the x-ray source. The analyzer was operated at a constant pass energy of 50 eV with a resolution of ~ 0.1 eV. Prior to the measurements, the surface of the samples was sputtered in-situ wwith an argon-ion beam to remove surface contamination.

The XPS Te $3d^{5/2}$ spectra for the glassy and crystallized FS and VD beads are shown in Fig. 18. The Te $3d^{5/2}$ binding energies obtained from Fig. 18 for different samples are given in Table 3 and compared to those for the standard crystalline forms of TeO_2 and TeO_3. Table 3 shows that the measured values of Te $3d^{5/2}$ binding energy for the FS glass beads and its crystalline form are within the Te $3d^{5/2}$ binding energy range for the crystalline TeO_2 standard, whereas, those for the VD glass beads and its crystalline form are within the Te $3d^{5/2}$ binding energy range for the crystalline TeO_3 standard. These results suggest

15

that the composition and structure of the FS beads are most likely different from those of the VD beads. The FS beads has a composition and structure close to those of α-TeO$_2$ and the VD beads has a composition and structure close to those of TeO$_3$. It is also likely that both samples, FS beads and VD beads, contain a mixture of TeO$_2$ and TeO$_3$ with FS beads containing a larger proportion of TeO$_2$ and VD beads containing a larger proportion of TeO$_3$. This result supports the previously observed DSC and XRD results for these samples, see section 3.2.1. A noticeable difference was observed in the DSC thermograms for the glassy FS and VD beads (Fig. 11) and in the XRD patterns for the crystallized FS and VD beads (Fig. 13). While the XRD pattern for the crystallized FS beads was identified as that of crystalline α-TeO$_2$, the pattern for the crystallized VD beads could not be identified.

3.2.4. Other Selected Properties:

A few other selected properties such as the refractive index, chemical durability, and specific heat of the glass beads prepared by flame spraying (FS beads) were measured. Due to an insufficient amount of samplet, these properties for the vapor deposited glass beads (VD beads) could not be measured.

3.2.4.1. Refractive index. The refractive index, n, of the glassy FS beads (~ 50 μm diameter) was measured using the Becke Line technique at 589.3 nm at 25°C. In the Becke Line method, small particles of a solid whose refractive index is to be measured, are immersed in liquids of known refractive index. When viewed with a microscope and the focus is raised, a faint band of light surrounding the particle enters the medium of higher refractive index, be it the solid or the liquid. By repeating the process systematically with liquids of incremental refractive index, the refractive index of the solid can be matched with the refractive index of the calibrated liquid or falls between two liquids. Based on measurements of 12 different beads, the refractive index of the FS glass beads was determined to be 2.166 ± 0.005 which is about twice of that for the most common silicate glasses.

3.2.4.2. Chemical Durability: The chemical durability of the FS glass beads was determined from measurements of their dissolution rate (DR) in deionized water at 25°C. A large value of DR indicates a poor chemical durability of the glass. The glass beads (about 1 g) were weighed with an accuracy of ±0.01 mg and

16

then immersed in about 100 cc of deionized water contained in a polythelene bottle for 1, 3, 7, 10 and 50 days. The bottles containing the glass beads and water were gently agitated once every day. After completion of the preset time, the water was removed and the beads were washed with acetone. The beads were then carefully weighed after drying at 80°C for 12 hours. The dissolution rate of the beads was determined from the difference in the initial and final weight, ΔW, as:

$$DR = \Delta W / (S * t) \quad (g/cm^2/min) \quad \ldots \quad \ldots \quad \ldots \quad (2)$$

where, S is the total surface area of all the beads in cm^2 and t is the time in min for which the beads were immeresed in water. S was calculated as:

$$S = 3W / (r * d) \quad \quad \ldots \quad \ldots \quad \ldots \quad (3)$$

where, W is the initial weight, d is the density, and r is the average radius of the glass beads. The density of the glass beads was assumed to be the same as that of the crystalline TeO_2, 5.67 g/cm^3. As analyzed by SEM (Fig. 9A), the diameter of the beads used for these measurements ranged from 45 to 75 μm. The average radius, r, of the beads was then calculated to be $(45 + 75)/4 \sim 30$ μm.

The weight loss per cm^2 of the glass beads is shown in Fig. 20 as a function of time. The slope of the staight line in Fig. 19 yields the average DR for the glass beads as $7 * 10^{-6}$ $g/cm^2/day$ or $4.71 * 10^{-9}$ $g/cm^2/min$ which is comparable to that of soda-lime-silica window glass and is considered an excellent chemical durability. The DR for the glass beads was also determined at the end of each time interval for which the beads were immersed in water and is shown in Fig. 20 along with the average DR (solid line) determined from Fig. 19. Fig. 20 shows that the chemical durability (in water) of these glass beads is independent of time and is the same as that determined from the slope in Fig. 19.

SEM photographs of the glass beads that were exposed to the ambient atmosphere for 7 days and which were immersed in deionized water for 2 days are shown in Fig. 21. The surface morphology of the beads in Fig. 21A which were exposed to the atmosphere for 7 days did not change significantly from that of the as-made beads, compare with Fig. 9A. This suggests that these TeO_2 glass beads havea good chemical resistance to the ambient atmosphere. However, the surface of the glass beads became very rough when immersed in deionized water

17

for 2 days, see Fig. 21B. Immersion in deionized water for 2 days totally changed the surface morphology of the beads, from very smooth (Fig. 9A or 21A) to very rough (Fig. 21B), suggesting these glass beads to have a low chemical durability in water. This result is opposite to what has been observed above (Figs. 19 and 20) from weight loss measurements.

The reasons for obtaining opposite results from two different measurements are presently unknown. The EDAX analysis of the corroded beads shows the presence of only Te. XRD analysis of these beads indicates that they are no amorphous any more, but contain crystals of α-TeO_2, see Fig. 22. This means that these TeO_2 glass beads crystallized to α-TeO_2 when in contact with water. In other words, the SEM photograph in Fig. 21B does not represent corrosion of the glass beads by water, rather it shows the glass to crystal transformations of the beads in presence of water. After being transformed to crystalline TeO_2, the beads remained highly durable as indicated by their weight loss, Figs. 19 and 20.

3.2.4.3. Specific Heat: The specific heat, c_p, of the FS glass beads was measured using differential scanning calorimetry (DSC-4, Perkin-Elmer, Norwalk, CT) at a heating rate of 20° C/min for a sample weighing 19.6 mg. The diameter of the glass beads was between 45 and 75 μm. Since the crystallization temperature for these glass beads is about 270°C, see Fig. 11, the specific heat of these beads was measured up to a maximum temperature of 250°C. No glass transition was observed in either the specific heat-temperature plot or the DSC thermogram in Fig. 11 for this TeO_2 glass. The specific heat for the TeO_2 glass was found to be constant at 106 ± 1.6 mcal/g/deg (70 J/mol/deg) from 120° to 250°C.

3.3. Sodium Tellurite Glasses:

The glass formation, crystallization, and structure of binary Na_2O-TeO_2 glasses were investigated as a function of composition by DSC, XRD, and IR spectra. A total of six glasses with TeO_2/Na_2O molar ratio of 2 (NT_2), 3 (NT_3), 4 (NT_4), 5 (NT_5) and 6 (NT_6) were prepared and studied in this investigation.

For DSC measurements, about 20 mg of glass powder composed of ~ 100 μm particles was sealed in an aluminum pan, which was then heated at 10°C/min in an atmosphere of flowing nitrogen gas until crystallization was complete. The DSC crystallization thermograms for the five (NT_2, NT_3, NT_4, NT_5, and NT_6) glasses are shown in Fig. 23. With the exception of the NT_4 glass, which has

18

only one crystallization peak, all other glasses exhibit multiple crystallization peaks, indicating crystallization of two or more phases.

The onset temperature for crystallization is also highest for the NT_4 glass, which indicates that the NT_4 glass is the most stable of those measured. When these glasses were kept in the ambient atmosphere, all but the NT_4 glass were found to be severley attacked by the moisture forming a white crystalline layer on the surface in less than 24 h. No change in color or appearance was observed for the NT_4 glass even after 30 days.

These sodium tellurite glasses were crystallized at the maximum temperature indicated by their respective DSC thermograms (Fig. 23) for 24 h and then analyzed by XRD. The crystals identified in each devitrified glass are listed in Table 4 along with the temperatures at which the glasses were crystallized. The crystalline phase(s) formed in each glass are in accordance with the phase diagram[18] for the binary Na_2O-TeO_2 system, with the exception that in the devitrified NT_3 glass both NT_4 and NT_2 crystals should be present according to the phase diagram, while only NT_4 crystals were identified in this sample.

Table 4 shows that the final crystallization products for these glasses contain only one or two crystalline phases, but the DSC thermograms (Fig. 23) for each glass (except the NT_4) exhibit more than two crystallization peaks. It appears, therefore, that the crystalline phases undergo a series of transformations during heating.

The IR spectra for these sodium tellurite glasses and their devitrified counterparts were measured using the KBr pellet technique. Analyses of these spectra show that the structure of the NT_4 glass contains both $[TeO_4]$ triangular bipyramidal (tbp) and $[TeO_3]$ triangular pyramidal (tp) groups, the $[TeO_4]$ groups being the primary structural units. The structure of the other glasses of higher or lower TeO_2 content than the NT_4 glass, contains a higher concentration of $[TeO_3]$ groups than that of the NT_4 glass. These results are in agreement with the results reported[19-22] previously from IR and Raman measurements that the basic structural units of the tellurite glasses are the $[TeO_4]$ tbp and $[TeO_3]$ tp groups.

Since the NT_4 glass was found to be the most stable and chemically durable of all the glasses in this binary sodium tellurite system, this glass was used for further investigation and property measurements.

3.3.1. Nucleation and Crystallization Kinetics:

The activation energy for crystallization, E, for the NT_4 glass was determined

using eqn. (1) (Section 3.1.4) and differential scanning calorimetry (DSC). Glass particles of 35 to 45μm and DSC heating rates of 2.5, 5, 7.5, 15, 20, 25, 30, 35, and 40 °C/min were used for the measurements. The Kissinger plot for the NT_4 glass, which is a straight line, is shown in Fig. 24. The slope of this straight line yields a value of E of about 268 ± 10 kJ/mol for this NT_4 glass, which is lower than that of $Li_2O.2SiO_2$ (about 300 kJ/mol), $Na_2O.2CaO.3SiO_2$ (about 370 kJ/mol), and $PbO.Bi_2O_3.Ga_2O_3$ (about 470 kJ/mol) glasses, see section 3.1.4. The lower value of E for the NT_4 glass probably indicates that the crystallization tendency for the NT_4 melt is higher than that of the lithium-disilicate, soda-lime-silicate, or lead-bismuth-gallate melts. The heat of crystallization (heat evolved during crystallization) was nearly independent of the DSC heating rate and was 230 ± 15 J/g.

The mechanism of crystallization (internal or surface) for the NT_4 glass was also determined from measurements of $(\delta T)_p$ and $T_p^2/(\Delta T)_p$ as a function of the glass particle size, see section 3.1.4 for discussion. The plots of $(\delta T)_p$ and $T_p^2/(\Delta T)_p$ as a function of particle size are shown in Fig.25 for the NT_4 glass where the amount of glass sample and DSC heating rate were kept constant at 40 mg and 15°C/min, respectively. Both $(\delta T)_p$ and $T_p^2/(\Delta T)_p$ decrease with increasing particle size (Fig. 25), which indicates that the NT_4 glass crystallizes primarily by surface crystallization.

3.3.2. Specific Heat:

The specific heat, c_p, for the NT_4 glass was first measured as a function of particle size using DSC at a heating rate (ϕ) of 20°C/min and was found to be independent of the glass particle size. The c_p-temperature curves for samples of different particle size were indistinguishable from each other. A representative c_p versus temperature curve for a sample composed of 425 to 500 μm particles measured at a heating rate of 20° C/min, is shown in Fig. 26. The glass transition region for this NT_4 glass ranges from about 250 (T_{g1}, lower glass transition temperature) to 270°C (T_{g2}, upper glass transition temperature) with T_g (average glass transition temperature) at about 260°C. The specific heat below the glass transition region, $c_p(g)$, is about 130 mcal/g/deg (76 J/mol/deg), whereas, above the glass transition region, $c_p(l)$ is about 207 mcal/g/deg (121 J/mol/deg).

The c_p for this glass, however, depended on the heating rate and the c_p measured at heating rates (ϕ) of 5, 10, 20, 30, and 40°C/min using a particle size

between 120 and 166 μm (average particle size of 143 μm) is shown in Fig. 27. The values for $c_p(g)$, $c_p(l)$, and T_g obtained from these curves (Fig. 27) are given in Table 5. It is clearly evident from Fig. 27 (and also from Table 5) that T_g increases with increasing ϕ. T_g and ϕ are related[23] as:

$$\ln \phi = - E_g/R \, (1/T_g) + const. \quad \text{...} \quad \text{...} \quad \text{...} \quad (4)$$

where E_g is the activation energy for glass transition. As expected from eqn. (4), a plot of $\ln\phi$ vs $1/T_g$ for the NT_4 glass produces a straight line, see Fig. 28, the slope of which yields an E_g of about 530 ± 10 kJ/mol.

It has been reported[23] that a dimensionless quantity, C, given by

$$C = (E_g/R) \, \Delta(1/T_g) \quad \text{...} \quad \text{...} \quad \text{...} \quad \text{...} \quad \text{...} \quad (5)$$

where, $\Delta(1/T_g) = (1/T_{g1} - 1/T_{g2})$, has nearly a constant value of about 4.8 for most glasses. An exception was noted for elemental Se and fused nitrate ($40Ca(NO_3)_2 - 60KNO_3$, mol%) glasses where the value of C was 10 and 9, respectively. The value of C in Table 5 for the NT_4 glass shows that there is a tendency for C to increase slightly with increasing heating rate. The average value of C for all the heating rates is about 4.0 ± 0.2 which is close to the predicted value of 4.8.

3.3.3. Evaporation Experiments in Low Gravity Drop Shaft:

The University of Missouri-Rolla (UMR) and the Osaka National Research Institute (ONRI), Japan jointly conducted several experiments on the evaporation of the NT_4 melt in low gravity using the drop shaft at the Japan Microgravity Center (JAMIC). This drop shaft is presently the world's longest (~ 710 m) and it is possible to attain ~ 10^{-4} g for 10 s during free-fall. The growth of solid particles from the vapor of this melt and the solidification of the melt remaining after evaporation were of primary interest.

Studies on the growth of solid particles from vapor in low gravity might provide new and important information on the kinetics of nucleation and growth for vapor-solid phase transformations. A low gravity environment where the motion of the evaporating species is not disturbed by gravity-driven convection would be a better environment for conducting these experiments. The evaporating species may form particles of more uniform size and sphericity in the

21

absence of convection in low gravity than particles condensed from vapor at 1-g. Particles of uniform size and sphericity have the potential for fabricating advanced materials of higher performance or in medicine as radiation delivery vehicles[24,25].

Investigation of the solidification of the melt remaining after evaporation will provide information on the nucleation, crystal growth, and glass forming ability for this melt in low gravity. This work was funded by UMR, the Government of Japan through different organizations, namely, Japan Space Utilization Promotion Center (JSUP), Science and Technology Agency (STA), and Agency of Industrial Science and Technology (AIST), and, partially, by NASA.

The experiments consisted of melting, evaporating and solidifying about 40 mg of a NT_4 glass adhered to a platinum heater coil during low gravity free-fall in the JAMIC drop shaft. The experiments were conducted in air at one atmosphere pressure. The heater coil which was ~ 5 mm long and 2 mm in internal diameter, was made from a 0.3 mm diameter platinum wire. The coil holding the glass was placed at the approximate center of rectangular glass box that was used to trap the species evaporated from the melt. A video camera and a 35 mm camera were used to record the entire evaporation event.

The species evaporating species from this NT_4 melt formed a near stagnant, spherical cloud of particles surrounding the melt in low-g, which grew to a diameter of ~ 2.8 cm in 10 seconds of low gravity. The cloud was destroyed during the high gravity (8-10 g) braking of the capsule. No such stagnant, spherical cloud pattern formed in similar experiments conducted 1-g due to gravity-driven convection. At 1-g, the cloud of condensed particles moved continuously upwards due to thermal convection. The condensed particles formed in low-g (from vapor) were smooth, spheres with a diameter ranging from 1 to 10 μm. They were about 4 to 5 times larger than similar spherical particles grown at 1-g. As analyzed by SEM, EDAX, and XPS, the chemical composition of these condensed particles was pure TeO_2. The spheres condensed from the vapor of the NT_4 melt were identified as chemically identical to the VD beads (prepared from the vapor of TeO_2 melt) discussed in section 3.2.

The melt remaining after evaporation (in low-g) was splattered on the bottom plate of the glass box that surrounded the heater coil holding the melt. These small splatters were completely crystallized and their composition was indistiguishable from that of the NT_4 glass used for these experiments. The complete crystallization of the splatters in the drop shaft experiments is a

22

surprising result, since this sodium-tellurite melt does not easily crystallize at 1-g. *A technical paper (Proc. Nineteenth Intl. Symp. on Space Technology & Science, 1994, pp. 651-56) that describes, in detail, the apparatus, experimental procedures and parameters, and the results for these low gravity drop shaft experiments is attached in Appendix 3.*

3.4. PbO-Nb$_2$O$_5$-TeO$_2$ Glasses:

A new class of optical glasses in the system PbO-Nb$_2$O$_5$-TeO$_2$ (PNT) has been developed primarily for use in ultrafast, all-optical switching devices. The glass forming area in this system as determined by melting a 10 g batch in a gold crucible between 750 and 1000°C for 20 to 40 min and quenching the melt onto a steel plate, is shown in Fig. 29. Since significant volatilization of TeO$_2$ occurs above 1000°C, compositions requiring a melting temperature above 1000°C were not investigated. The glasses had a slight yellow color, but the color was much less than the glasses containing PbO, Bi$_2$O$_3$, and Ga$_2$O$_3$ (see Section 3.1), which have been considered excellent nonlinear optical glasses up to this time.

The physical, thermal, and chemical properties such as the density, molar volume, thermal expansion coefficient, dissolution rate in solutions of different pH, softening, glass transition, and crystallization temperatures, and the transmission in the UV-Visible (350 to 750 nm) and IR (1 to 22 μm) were measured as a function of composition for the glasses located in the shaded area in Fig. 29 in order to determine their suitability for practical use. The analyses of the IR spectra as measured by the Kbr pellet technique from 450 to 1400 cm^{-1} suggest that like the sodium-tellurite glasses (section 3.3), the structure of these PNT glasses also contains [TeO$_4$] tbp and [TeO$_3$] tp in several forms such as chains, islands, and isolated [TeO$_4$] and [TeO$_3$] groups. The Nb^{5+} ions in these glasses are believed to take part in the network by replacing the Te-O-Te bonds by Te-O-Nb bonds, which results in an improvement in glass formation and properties for the glasses containing a higher concentration of Nb$_2$O$_5$. PbO in these glasses acts primarily as a network modifier with Pb^{2+} ions occupying the interstitial positions in the glass network.

The glass formation, structure, and properties for the PNT glasses have been reported in two technical papers (Proc. XVII Intl. Cong. on Glass, vol. 5, p. 395, 1995 and J. Shanghai Inst. Building Materials, vol. 8, no. 4, p. 291, 1995) which are enclosed with the present report as Appendix 4. The physical, thermal, chemical, and optical properties for the PNT and lead-bismuth-gallate

23

(section 3.1) glasses have been compared also in these papers. Comparison of a few selected properties between one glass from each system ($10PbO$-$20NbO_{2.5}$-$70TeO_2$ (PNT-7) and $40PbO$-$35BiO_{1.5}$-$25GaO_{1.5}$ (HMO-7 in Table 1), cat%) is shown in Table 6 as an example.

Table 6 shows that most of those properties that are critical for practical use are superior for the PNT-7 glass compared to those for the HMO-7 glass. For example, the PNT-7 glass is more resistant to crystallization (higher crystallization temperature, T_c) and is more chemically durable (lower dissolution rate, DR, value) than the HMO-7 glass. A higher value of the thermal expansion coefficient, α, for the PNT-7 glass makes it more useful for glass to metal seals and a lower value of the cut off wavelength in the ultraviolet-visible, $\lambda_{UV\text{-}VIS}$, makes it less colored than the HMO-7 glass. Most important is the coefficient of non-linear refractive index, n_2, which has been determined for the PNT-7 and HMO-7 glasses using the empirical relation[26]

$$n_2 = (391 \times 10^{-13})\,(n\text{-}1)/v^{5/4} \qquad \dots \qquad \dots \qquad \dots \qquad (6)$$

and their measured linear refractive index, n, as a function of wavelength. The typical linear refractive index measured for the PNT-7 glass as a function of wavelength from 250 to 850 nm using an ellipsometer is shown in Fig. 30. The value of n_2 for the PNT-7 glass is about 18.4×10^{-13} esu (Table 6) which is almost twice the 10.6×10^{-13} esu value for the HMO-7 glass. A higher value of n_2 for the PNT-7 glass should cause it to be a faster optical switch and makes it a better nonlinear optical glass than the HMO-7 glass.

4. Conclusions:

The present research has led to the following conclusions.

A. *PbO-Bi₂O₃-Ga₂O₃ Glasses:*

1. Attempts, including containerless melting, to decolorize these lead-bismuth-gallate glasses were not completely successful in totally eliminating the color of these glasses. The light yellow color is believed to be intrinsic to these glasses and to be associated with the combined presence of lead and bismuth ions. Melting these glasses in a platinum crucible or in an oxygen-rich atmosphere causes the

24

color to become more intense. Melting in nitrogen or air atmospheres and in a gold or alumina crucible yielded glasses having the least color (pale yellow).

2. Melting at 900°C for 30 min minimizes the loss of lead and bismuth by volatilization and produces a homogeneous, cord- free and bubble-free glass.

3. The density, molar volume, thermal expansion coefficient, glass transtion and crystallization temperatures, and the transmission in the UV, Visible, and IR measured in the present work for the lead-bismuth-gallate glasses as a function of composition are in excellent agreement with previously reported values. The chemical durability of these glasses, which has not been reported before, is comparable to that of the soda-lime-silica window glass, especially when the amount of PbO content is low, 20 to 30 cat%.

4. Analyses of the preceding property data suggest that Ga^{3+} improves glass formation and acts primarily as a network forming cation in these glasses, possibly forming $[GaO_4]$ tetrahedra in the glass structure. The majority of the lead and bismuth ions are believed to act as network modifiers, suppressing the tendency for glass formation as a whole.

5. The thermal expansion coefficient and glass transition temperature data also suggest that the lead ions in these glasses exist as both Pb^{2+} and Pb^{4+}, the proportion of Pb^{4+} being about 10%. This result is further supported by the weight loss which occurred during melting when the Pb_3O_4 used in the glass batch is believed to decompose to PbO, PbO_2, and O_2 . Since the presence of cations with +3 or higher charge generally favors glass formation, it is, therefore, likely that some of the Pb^{4+} ions might occupy network-forming sites in the glass structure.

6. The DTA, TGA, and XRD analyses show that when the glasses containing a high amount of Bi_2O_3 (40 to 60 cat%) are heated in oxygen (or air) above their crystallization temperatures (generally above 500°C), they undergo a phase transformation involving the oxidation process of Pb^{2+} to Pb^{4+}. In this process a portion of the $2PbO.3Bi_2O_3$ phase that initially formed during crystallization is converted to $2PbO_2.12Bi_2O_3$. The conclusions in (4) through (6) were

25

also confirmed by IR and Raman measurements.

7. Using DTA technique the following information was obtained for a $60PbO.10BiO_{1.5}.30GaO_{1.5}$, cat%, glass.

   (i) The activation energy for crystallization is about 470 ± 15 kJ/mol.

   (ii) The temperature where nucleation can occur in this glass ranges from 265° to 375°C.

   (iii) The temperature where the nucleation rate is a maximum is 343 ± 5°C.

   (iv) This glass crystallizes primarily by surface crystallization.

B. TeO_2 Glass:

1. Pure TeO_2 glass was prepared in large quantities (several gms) for the first time using a flame fusion technique and commercially available TeO_2 powders . This TeO_2 glass was prepared in the form of small spherical beads with a maximum diameter of about 75 μm, which will be referred to as FS beads to differentiate them from another kind of glass beads formed from the condensation of vapor of the TeO_2 melt. The latter kind which had a maximum diameter of about 1 μm, will be called VD beads.

2. Analysis by differential scanning calorimetry (DSC) shows that the VD beads crystallize at a higher temeprature, have a higher activation energy for crystallization, and a smaller DSC peak area than those for the FS beads. All these results suggest that the VD beads are more resistant to crystallization than the FS beads.

3. X-ray diffraction (XRD) patterns for the crystallized FS beads and VD beads were totally different. The crystallized FS beads contained crystalline α-TeO_2 (paratellurite), while the phase(s) in crystallized VD beads could not be identified.

4. Analysis of Te $3d^{5/2}$ binding energy for the FS beads and VD beads by x-ray photoelectron spectroscopy (XPS) suggest that the chemical composition and structure of the FS beads are similar to those of TeO_2, whereas, the composition and structure of the VD beads are similar to those of TeO_3. However, the IR and Raman spectra for these two type of beads showed no difference.

5. Other selected properties such as the refractive index, n, chemical durability (in deionized water), DR, and specific heat, c_p, were measured for the glassy FS beads. These properties for the VD beads could not be measured due to insufficient sample. The refractive index, n, for the FS beads at 583 nm and 25° C, was 2.166 ± 0.005. This is significantly higher than the 1.48 to 1.56 index for most of the silicate glasses. When immersed in deionized water for 24 h, these glass beads crystallized to α-TeO$_2$, but the average DR remained as high as 4.7 * 10^{-9} g/cm^2/min. This DR is comparable to that of soda-lime-silica window glass. The c_p for these glass beads, as measured by DSC at a heating rate of 20° C/min, was nearly constant from room temperature to the crystallization temperature at about 285°C and was about 70 J/mol/K.

C. Na$_2$O-TeO$_2$ Glasses:

1. The glass formation of Na$_2$O-TeO$_2$ glasses with Na$_2$O/TeO$_2$ molar ratio as 2 (NT$_2$), 3 (NT$_3$), 4 (NT$_4$), 5 (NT$_5$), and 6 (NT$_6$) was investigated using DSC and XRD. The NT$_4$ glass was found to have the least tendency to crystallize (highest glass formability) and highest chemical durability of all six glasses investigated.

2. The IR spectra for these glasses suggest that the structure of the NT$_4$ glass contains both [TeO$_4$] triangular bipyramid (tbp) and [TeO$_3$] triangular pyramid (tp) groups, the [TeO$_4$] groups being the primary structural units. The structure of all other glasses of higher and lower TeO$_2$ content than the NT$_4$ glass contains a higher concentration of [TeO$_3$] groups than the NT$_4$ glass.

3. The NT$_4$ glass was used for further property measurements, since this glass was the most stable of all the sodium-tellurite glasses. As determined by DSC, the NT$_4$ glass was found to crystallize primarily by surface crystallization with an overall activation energy for crystallization, E, of about 270 kJ/mol (E for a typical lithium-disilicate glass is about 300 kJ/mol and that for a pure TeO$_2$ glass is about 172 kJ/mol).
   Although the melting temperature for the NT$_4$ glass (~ 470° C) is

much lower than that of a TeO_2 glass (~ 732°C), the crystallization temperature for NT_4 (~ 350°C) was higher than that of pure TeO_2 glass (~ 288°C).

4. Unlike pure TeO_2 glass, the specific heat (c_p) temperature curve for the NT_4 glass showed a distinct glass transition which ranged from about 250 to 270°C with an average glass transition temperature (T_g) of about 260°C. The c_p below and above the glass transition region for the NT_4 glass was about 76 J/mol/K and 121 J/mol/K, respectively, which are higher than the average 70 J/mol/K c_p value for a TeO_2 glass. The activation energy for the glass transition, E_g, as determined from the measurements of c_p as a function of heating rate was about 530 kJ/mol.

5. When a small amount (~ 40 mg) of this NT_4 glass fused to a platinum heating coil was evaporated in low gravity (~ 10^{-4} g) for about 10 s in the world's longest drop shaft in Japan (JAMIC), the evaporating species formed a near stagnant, spherical cloud of spherical particles surrounding the melt. In similar experiments conducted at 1-g, no such near stagnant, spherical cloud of particles formed due to gravity-driven convection.

The particles condensed from the vapor in the low gravity experiments consisted of highly spherical, amorphous particles of TeO_x, whose average diameter was between 4 and 7 μm, with a maximum diameter of about 20 μm. The limited amount of sample made it impossible to confirm whether the chemical composition of these microspheres is TeO_2 or TeO_3. The average diameter of these TeO_x microspheres made in 10^{-4} g was 5 to 6 times larger than the TeO_x particles grown from similar experiments at 1-g.

The melt remaining after evaporation, which was splattered on glass plates, crystallized completely and its chemical composition was indistinguishable from that of the starting NT_4 glass. This crystallization is particularly interesting, since this NT_4 glass cannot be easily crystallized when melted at 1-g. Why a small amount of an NT_4 melt which is an excellent glass former at 1-g, crystallized rapidly when cooled at an estimated rate of 1000° C/sec in low

28

gravity is not easily understood at this time and warrants further investigation.

D. PbO-Nb₂O₅-TeO₂ Glasses:

1. A new class of optical glasses based on PbO, Nb_2O_5, and TeO_2 (PNT) has been developed primarily for non-linear optical (NLO) applications such as in ultrafast, all optical switching devices. The physical, thermal, and chemical properties of these PNT glasses are superior to those of the $PbO-Bi_2O_3-Ga_2O_3$ (HMO) glasses that are considered excellent NLO glasses up to this time. Also, the coefficient of non-linear refractive index, n_2, for a PNT glass is nearly double of that for a HMO glass ($n_2 = 18.4 \times 10^{-13}$ esu for the PNT glass compared to 10.6×10^{-13} esu for the HMO glass). A higher value of n_2 ensures a faster response in optical switching devices.

2. The analysis of the IR spectra for the PNT glasses suggests that the structure of these glasses consists of primarily chains, islands, and isolated $[TeO_4]$ (triangular bipyramid) and $[TeO_3]$ (triangular pyramid) groups. $[NbO_6]$ groups connect the chains or islands of $[TeO_4]$ or $[TeO_3]$ groups and increase the cross link density in the structure, thereby, making the glasses more stable and chemically durable. The PbO most likely acts like a net work modifier in these glasses with the Pb^{2+} ions occupying the interstitial positions in the glass network.

E. Spin-off: Identifying internal and surface crystallization by DTA/DSC for the glass to crystal transformations.

One of the most significant and, perhaps, lasting outcomes of this research is that a rapid and convenient method, based on DTA/DSC has been developed which allows internal crystallization to be distinguished from surface crystallization occuring in glasses. Knowledge of the crystallization mechanism (internal or surface) operating in a particular glass is critically important to controlling the processing parameters for producing glass-ceramics of desired properties. This DTA/DSC technique, which has been shown to be theoretically justified and which has been widely accepted as an

29

alternative and rapid method for identifying internal and surface crystallization, requires only a few (6 to 8) DTA/DSC scans at a fixed heating rate as a function of size of the glass particles. The primary crystallization mechanism in several glasses in the system Li_2O-SiO_2, $BaO-SiO_2$, $Na_2O-CaO-SiO_2$, $PbO-Bi_2O_3-Ga_2O_3$, Na_2O-TeO_2 and $PbO-Nb_2O_5-TeO_2$ was investigated using the present technique. The results were confirmed by directly observing the microstructure of the crystallized samples by SEM, *see #16, 17, 18 and 20 in the list of publications supported by the present contract.* The DTA/DSC technique is believed to have universal application to all types of oxide glasses.

References:

1. E. M. Vogel, *J. Am. Ceram. Soc.*, **72**, 719 (1989).

2. W. H. Daumbaugh and J. C. Lapp, *J. Am. Ceram. Soc.*, **75**, 2315 (1992).

3. T. Komatsu, H. Tawarayama, H. Mohri and K. Matusita, *J. Non-Cryst. Solids*, **135**, 105 (1991).

4. J. C. Lapp, W. H. Daumbaugh, and M. L. Powley, *Riv. Stn. Sper. Vetro (Murano, Italy)*, **19**, 91 (1989).

5. H. Nasu, O. Matushita, K. Kamiya, K. Kobayashi and K. Kubodera, *J. Non-Cryst. Solids*, **124**, 275 (1990).

6. C. Zhu, X. Lu, and Z. Zhang, *J. Non-Cryst. Solids*, **144**, 89 (1992).

7. H. Burger, K. Kneipp, H. Hobert and W. Vogel, *J. Non-Cryst. Solids*, **151**, 134 (1992).

8. M. M. Abouelleil and F. J. Leonberger, *J. Am. Ceram. Soc.*, **72**, 1311 (1989).

9. H. E. Kissinger, *J. Res. Natl. Bur. Stand. (US)*, **57**, 217 (1956).

10. C. S. Ray and D. E. Day, *Cer. Trans*, **30**, 207 (1993).

11. X. J. Xu, C. S. Ray, and D. E. Day, *J. Am. Ceram. Soc.*, **74**, 909 (1991).

12. C. S. Ray and D. E. Day, *J. Am. Ceram. Soc.*, **73**, 439 (1990).

13. C. S. Ray and D. E. Day, *Thermochimica Acta*, **280 & 281**, 163 (1996).

14. D. E. Day, *US Patent # 4, 789, 501: 5, 302, 369.*

15. W. Huang, C. S. Ray, and D. E. Day, *J. Am. Ceram. Soc.*, **76**, 865 (1993).

16. C. S. Ray, M. Makihara, J. Hayakawa and D. E. Day, *Proceedings of the noneteenth International Symposium on Space Technology and Science*, pp. 651-56, 1994.

17. T. Sekiya, N. Mochida, A. Ohtsuka and M. Tonokawa, *Nippon Seramikkusu Kyokai Gakujutsu Ronbunshi*, **97**, 1435 (1989).

18. B. P. Troitskii, O. K. Yakhkind, and N. S. Martyshchenko, *Inorganic Materials*, **3**, 661 (1967) (Translated in English from Russian).

19. Y. Dimitriev, V. Dimitriov, and M. Arnaudov, *J. Mater. Science*, **14**, 723 (1979); **18**, 1353 (1983).

20. T. Sekiya, N. Mochida, A. Ohtsuka and M. Tonokawa, *Nippon Seramikkusu Kyokai Gakujutsu Ronbunshi*, **97**, 1435 (1989).

21. Y. Himei, A. Osaka, T. Namba and Y. Miura, *J. Non-Cryst. Solids*, **177**, 164 (1994).

22. M. Tatsumisago, S-K Lee, T. Minami and Y. Kowada, *J. Non-Cryst. Solids*, **177**, 154 (1994).

23. C. T. Moynihan, *J. Am. Ceram. Soc.*, **76**, 1081 (1993).

24. D. E. Day and G. H. Ehrhardt, *US Patent # 5, 011, 677 (30 April 1991).*

25. D. E. Day and T. E. Day, An Introduction to Bioceramics, Advanced Series in Ceramics (Eds. L. Hench and J. Wilson), Chapter 9, p. 305, World Series Publishing Company (1993).

26. N. L. Boling, A. J. Glass, and A. Owyoung, *IEEE J. Quantum Electronics*, **QE-14**, 601 (1978).

List of Publications Supported Partially or Fully by the Present Contract NAGW-2846.

1. Evaporation and Convection from Glass Melts Under Low- and High-g: Drop Shaft and Aircraft Experiments: M. Makihara, J. Hayakawa, C. S. Ray and D. E. Day, *Japan Society for Microgravity Applications (JASMA)*, **9**, 186-194 (1992).

2. Results of Demonstration Experiments at the Japan Microgravity Center (JAMIC): Use of Dropshaft to Process Photonic Materials: M. Makihara, J. Hayakawa, C. S. Ray and D. E. Day, *In Space '92 Symposium Proceedings*, 17-20 November (1992), Tokyo, Japan, pp. 53-65.

3. Nucleation and Crystallization in Glasses as Determined by DTA: C. S. Ray and D. E. Day, *Ceramic Transactions: Nucleation and Crystallization in Liquids and Glasses*, Ed. M. C. Weinberg, Vol 30, pp. 207-223, 1993. American Ceramic Society, Inc., westerville, OH.

4. Enhanced Formation of Calcia-Gallia Glass by Containerless Processing: J. K. R. Weber, D. R. Merkley, C. D. Anderson, P. C. Nordine, C. S. Ray and D. E. Day, *J. Am. Ceram. Soc.*, **76**, 2139-41 (1993).

5. Heavy Metal Oxide Glass, Part I. Preparation and Properties: W. Huang, C. S. Ray, and D. E. Day, *Glass & Enamel*, **21**, [4], 1-8 (1993) (in Chinese).

6. Heavy Metal Oxide Glass, Part II. Structural Aspect and Crystallization Behavior: W. Huang, C. S. Ray, and D. E. Day, *Glass & Enamel*, **21**, [6], 1-12 (1993) (in Chinese).

7. The Determination of Nucleation rate Curve in the Crystallization Process of Glasses from DTA Technique: W. Huang, C. S. Ray, and D. E. Day, *J. Shanghai Inst. Building Materials*, **6**, [3], 187-95

(1993) (in Chinese).

8. Color and Selected Properties of PbO-BiO$_{1.5}$-GaO$_{1.5}$ Glasses: W. Huang, C. S. Ray, and D. E. Day, *J. Am. Ceram. Soc.*, **77**, 1017-24 (1994).

9. Evaporation of Sodium Tellurite Melt in the JAMIC Low Gravity Drop Shaft: C. S. Ray, M. Makihara, J. Hayakawa and D. E. Day, *Proceedings of the Nineteenth International Symposium on Space Technology and Science*, 1994, pp. 651-56 (Yokohama, Japan, 15-24 May 1994).

10. Formation and Properties of PbO-NbO$_{2.5}$-TeO$_2$ Glasses: W. Huang, C. S. Ray, and D. E. Day, *Proceedings of the XVII International Congress on Glass*, **5**, 395 (1995).

11. Glass Microspheres Formed by Evaporating a Sodium Tellurite Melt in Low Gravity; MGLAB Drop Shaft Experiments: M. Makihara, J. Hayakawa, C. S. Ray and D. E. Day, *JASMA*, **12**, 267 (1995).

12. Application of Electric Properties to Research on Glass Crystallization Process: W. Huang, C. S. Ray, and D. E. Day, *J. Shanghai Inst. Building Materials*, **8**, [3], 193-202 (1995) (in Chinese).

13. Properties and Structure of PbO-NbO$_{2.5}$-TeO$_2$ Glasses: W. Huang, C. S. Ray, and D. E. Day, *J. Shanghai Inst. Building Materials*, **8**, [4], 291-301 (1995) (in Chinese).

14. Effect of Platinum Doping on Nucleation and Crystallization in Li$_2$O.2SiO$_2$ Glass; Experimental Measurements and Computer Modeling: K. L. Narayan, K. F. Kelton, C. S. Ray, *J. Non-Cryst. Solids*, **195**, 148-157 (1996).

15. Analysis of Properties of Nonlinear Optical Glass Containing Tellurite: W. Huang, C. S. Ray, and D. E. Day, *Glass & Enamel*,

35

24, [1], 1 (1996) (in Chinese).

16. Identifying Internal and Surface Crystallization by Differential Thermal Analysis for the Glass to Crystal Transformations: C. S. Ray and D. E. Day, *Thermochimica Acta*, **280 & 281**, 163-174 (1996).

17. Nonisothermal Calorimetric Studies of the Crystallization of Lithium Disilicate Glass: C. S. Ray, D. E. Day, W. Huang, K. L. Narayan, T. C. Cull and K. F. Kelton, *J. Non-Cryst. Solids (in press)*.

18. Computer Modeling of Nonisothermal Crystallization: K. F. Kelton, K. L. Narayan, L. E. Levine, T. C. Cull and C. S. Ray, *J. Non-Cryst. Solids (in press)*.

19. Raman Studies of $PbO-Bi_2O_3-Ga_2O_3$ Glasses: A. Mogus-Milankovic, K. Furic, W. Huang, C. S. Ray and D. E. Day, *Phys. & Chem. Of Glasses (in press)*.

20. Surface and Internal Crystallization in Glasses as Determined by DTA: C. S. Ray, W. Huang, Q. Yang and D. E. Day, *J. Am. Ceram. Soc. (in press)*.

21. The Analysis of Nucleation Rate Type Curves as Determined by DTA: C. S. Ray and D. E. Day, *J. Am. Ceram. Soc. (communicated)*.

Table 1. Density, Molar Volume, Average Thermal Expansion Coefficient, Glass Transition Temperature, Dissolution Rate and Cutoff Wavelength in UV-Visible and IR for $xPbO \cdot (100 - (x + y))BiO_{1.5} \cdot yGaO_{1.5}$(cat%) Glasses

Composition		Density, d (g/cm³)	Molar volume, V_m (cm³)	Thermal Expansion Coefficient, α (×10⁻⁷/°C)*	Glass Transition Temperature, T_g (°C)	Dissolution Rate, DR (g/(cm².min))[+]		Cutoff Wavelength	
x	y					pH 4	pH 10	λ_{VIS} (nm)	λ_{IR} (μm)
20	20	8.414	40.1 (40.0)	130	342	8.5×10^{-9}	5.4×10^{-9}	487	8.0
30	20	8.403	37.0 (37.5)	130	333	1.3×10^{-8}	4.4×10^{-8}	490	8.0
40	20	8.360	34.4 (35.0)	130	329	7.4×10^{-8}	4.4×10^{-8}	497	7.9
50	20	8.331	32.0 (32.5)	127	325	1.6×10^{-5}	1.3×10^{-5}	498	7.9
20	25	8.294 (8.250)	39.4	124	355	2.0×10^{-9}	2.7×10^{-9}	478	7.8
30	25	8.289	36.2	124	345	4.9×10^{-9}	2.9×10^{-9}	479	7.8
40	25	8.204	33.8	124	339 (325)	6.2×10^{-8}	3.2×10^{-6}	480	7.7
50	25	8.158	31.6	122	338 (325)	1.1×10^{-5}	1.2×10^{-5}	490	7.7
30	30	8.080	35.8	115 (110)	361 (350)	1.9×10^{-8}	9.6×10^{-7}	470	7.8
40	30	8.051 (8.000)	33.2	115 (110)	359 (350)	1.7×10^{-7}	5.7×10^{-6}	478	7.7
50	30	7.996 / 8.02±	31.0	114 (110)	359 (350) 347±	2.2×10^{-5}	8.4×10^{-5}	483	7.7
60	30	7.957	29.1	108	358 (350)	6.1×10^{-5}	6.7×10^{-5}	493	7.7
40	35	7.881 / 7.980±	32.7	111 (100)	379 364±	2.7×10^{-6}	6.4×10^{-6}	472	7.7
50	35	7.829	30.5	111 (100)	377	1.7×10^{-5}	2.8×10^{-5}	482	7.7
60	35	7.766 (7.750)	28.7	108	374	3.7×10^{-5}	7.4×10^{-5}	487	7.7

*Average between 25° and 250°C.   [+] Measured in HCl (pH 4.0) and NaOH (pH 10.0) at 25°C.   Values in parentheses are from Reference 4.   [+] J.A. Ruller and J.E. Shelby, Phys. Chem. Glasses, **33**, 177 (1992).

Table 2. Glass composition and the crystalline phases identified by XRD for the glasses crystallized in DTA

| Glass Sample | Composition (Cat %) | | | Crystalline Phases | | | |
| | PbO | $BiO_{1.5}$ | $GaO_{1.5}$ | XRD - 1* | | XRD - 2** | |
				Major	Minor	Major	Minor
HMO-1	20	60	20	PbO	PbO_x	3	1, 2
HMO-2	30	50	20	PbO	PbO_x	3	1, 2
HMO-3	40	40	20	PbO	PbO_x	3	1, 2
HMO-4	50	30	20	PbO	PbO_x	3	1, 2
HMO-5	20	55	25	PbO	PbO_x	3	1, 2
HMO-6	30	45	25	PbO	PbO_x	3	1, 2
HMO-7	40	35	25	PbO	PbO_x	3	1, 2
HMO-8	50	25	25	PbO	None	PbO	None
HMO-9	30	40	30	PbO	PbO_x	3	1, 2
HMO-10	40	30	30	PbO	PbO_x	3	1, 2
HMO-11	50	20	30	PbO	None	PbO	None
HMO-12	60	10	30	PbO	None	PbO	None
HMO-13	40	25	35	PbO	PbO_x	3	1, 2
HMO-14	50	15	35	PbO	None	PbO	None
HMO-15	60	5	35	PbO	None	PbO	None

* DTA terminated after the first crystallization peak (between 390 and 460°C depending upon samples), and the samples analyzed by XRD.
** DTA terminated at ~550°C and the samples analyzed by XRD. For PbO_x, $1 < x \leq 2$.

1: $2PbO \cdot 3Bi_2O_3$ 2: $4PbO \cdot 5Bi_2O_3$ 3: $2PbO_2 \cdot 12Bi_2O_3$

Table 3. Measured Te $3d^{5/2}$ binding energy in amorphous and crystalline TeO_2

TeO_2 Crystalline Standard* (ev)	TeO_3 Crystalline Standard* (ev)	Glass (FS Beads) (ev)	Crystalline (FS Beads) (ev)	Glass (VD Beads) (ev)	Crystalline (VD Beads) (ev)
575.8 - 576.2	576.8 - 577.3	575	576	577	577

* Handbook of X-ray Photoeletron Spectroscopy, Perkin Elmer Corporation, Physical Electronics Division (1979).

Table 4. Crystals identified by XRD in the crystallized sodium-tellurite glasses

Glass Composition	Crystallization Temperature, °C	Crystals Identified by XRD
NT_2	360	NT_2
NT_3	360	NT_2
NT_4	350	NT_4
NT_5	385	NT_4, TeO_2
NT_6	385	NT_4, TeO_2

NT_x: $Na_2O \cdot xTeO_2$, x = 2, 3, 4, 5 and 6

Table 5. Specific heat (c_p) and glass transition temperature (T_g) at different heating rates for an $Na_2O \cdot 4TeO_2$ (NT_4) glass with particle size between 170 and 290 μm.

Heating Rate ϕ, °C/min	T_g,K	$\Delta(T_g)$*,K	$c_p(g)$** mCal/g/deg	$c_p(l)$** mCal/g/deg	C***
5	529	16.3	114	82	3.8
10	531	16.9	127	81	3.9
20	534	17.7	125	80	3.9
30	537	18.7	124	83	4.1
40	538	19.0	126	85	4.2

*$\Delta(T_g)$:   Width of the glass transition region, $T_{g2} - T_{g1}$

**$c_p(g)$:   Sp. heat for glass below T_{g1}

   $c_p(l)$:   Sp. heat for liquid above T_{g2}

***C: A dimensionless quantity $= (E_g/R) (1/T_{g1} - 1/T_{g2})$, E_g being the activation energy for glass transition.

Note: T_g and $\Delta(T_g)$ increase with increasing ϕ, but $c_p(g)$ and $c_p(l)$ are nearly independent of ϕ.

Table 6. Comparison of Selected Properties for PNT and PBG Glasses

	PNT Glass*	PBG Glass**
d, g/cm³	5.75	8.20
α, 10⁻⁷/°C	158	124
T_g, °C	378	339
T_c, °C	436	409
DR at 25°C, g/cm⁻²•min (acid)	8.8×10^{-9} (pH 2)	6.2×10^{-8} (pH 4)
DR at 25°C, g/cm⁻²•min (alkali)	8.0×10^{-8} (pH 12)	3.2×10^{-6} (pH 10)
DR at 25°C, g/cm⁻²•min (deionized water)	$< 8.0 \times 10^{-10}$ (pH 7)	1.5×10^{-6} (pH 7)
λ_{UV-VIS}, nm	408	480
λ_{IR}, μm	5.6	7.7

* $10PbO \cdot 20NbO_{2.5} \cdot 70TeO_2$, cat%   ** $40PbO \cdot 35BiO_{1.5} \cdot 25GaO_{1.5}$, cat%
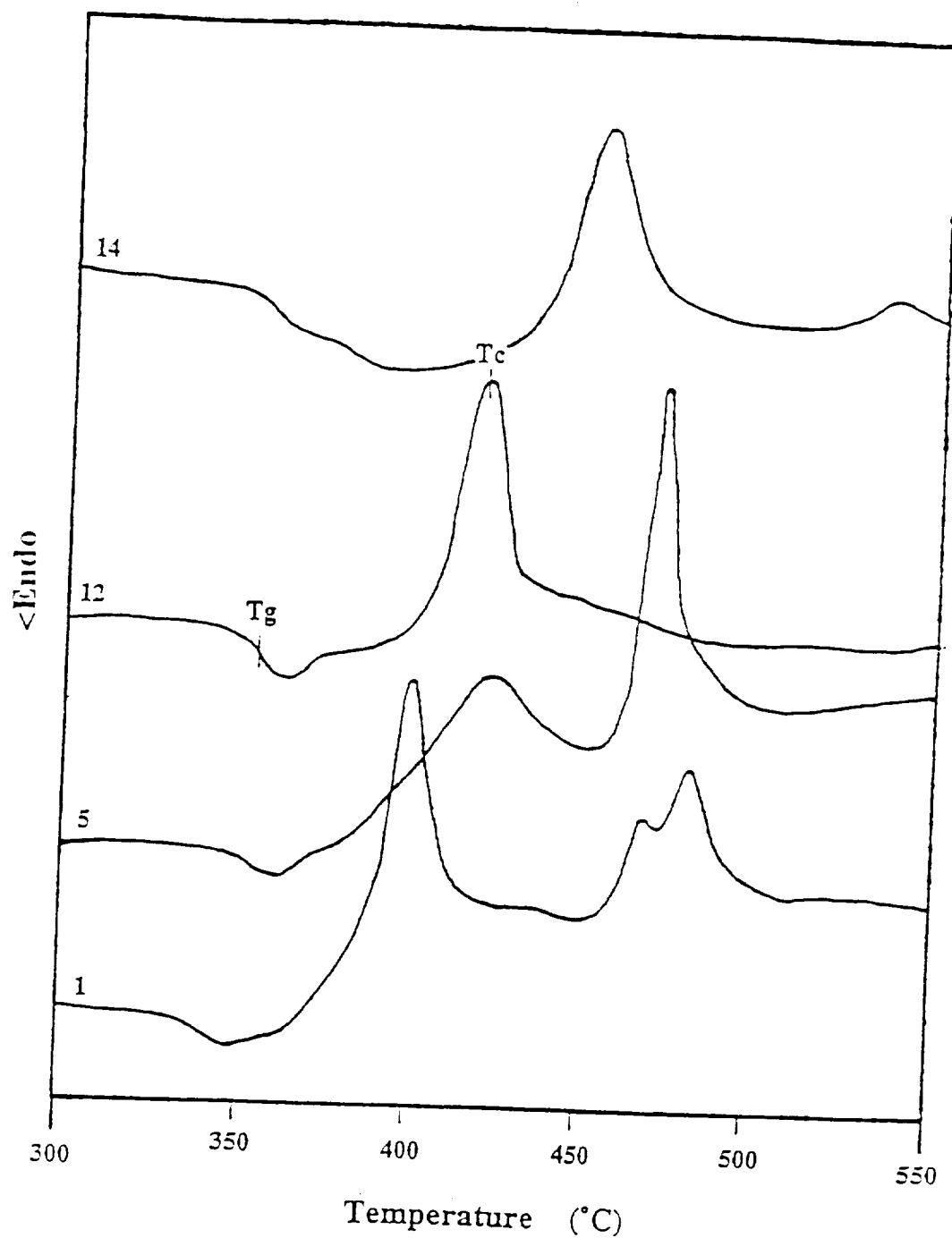
Fig. 1. DTA thermograms for four glasses in the system PbO-$BiO_{1.5}$-$GaO_{1.5}$. Sample weight: 60 mg, Particle size: <38 μm, Atmosphere: flowing nitrogen, DTA heating rate: $10°$ C/min. Glass composition (cat%): (1) $20PbO$-$60BiO_{1.5}$-$20GaO_{1.5}$, (5) $20PbO$-$55BiO_{1.5}$-$25GaO_{1.5}$, (12) $60PbO$-$10BiO_{1.5}$-$30GaO_{1.5}$, (14) $50PbO$-$15BiO_{1.5}$-$35GaO_{1.5}$.
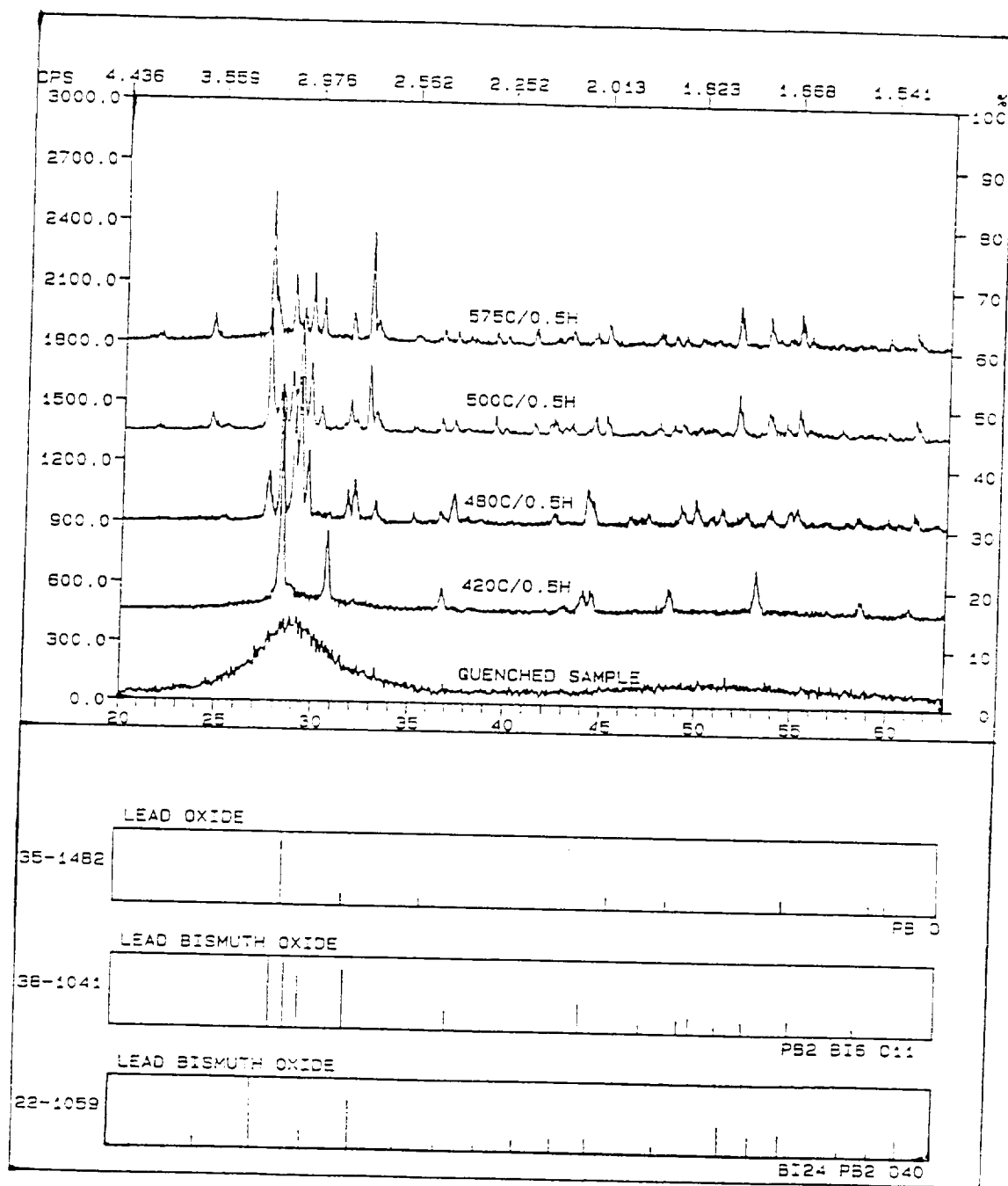
Fig. 2. The x-ray diffraction patterns at different temperatures (high temperature XRD) for a $20PbO-60BiO_{1.5}-20GaO_{1.5}$, cat%, glass (HMO-1, Table 2). With increasing temperature the primary crystalline phase changes from PbO to $2PbO.3Bi_2O_3$ to $2PbO_2.12Bi_2O_3$.
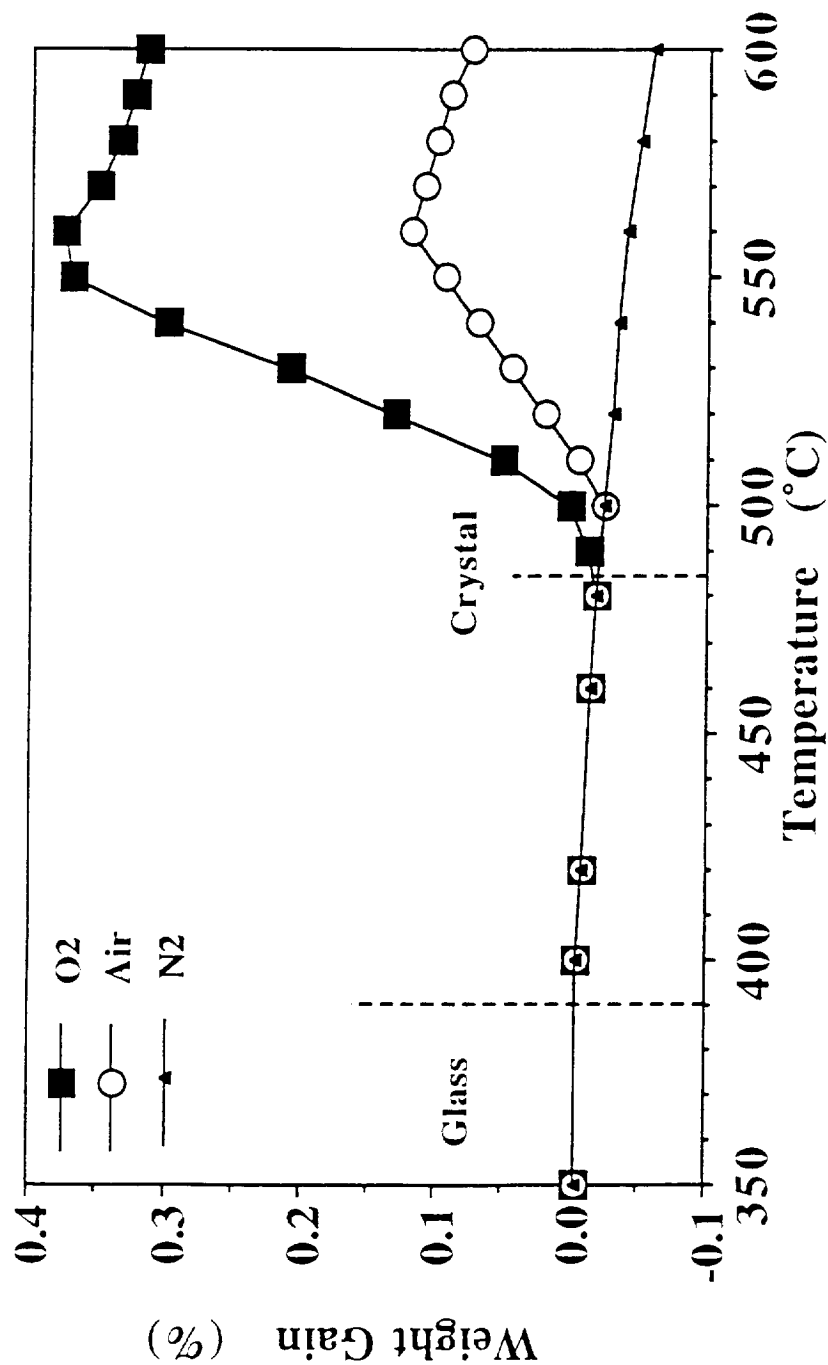
Fig. 3. Thermogravimetric analysis (TGA) for a 20PbO-60BiO$_{1.5}$-20GaO$_{1.5}$, cat%, glass (HMO-1, Table 2) in different atmospheres shown. A gain in sample weight is observed at about 500° C when the TGA is performed in either oxygen or air, but no such weight gain is observed in an oxygen-free atmosphere such as nitrogen.
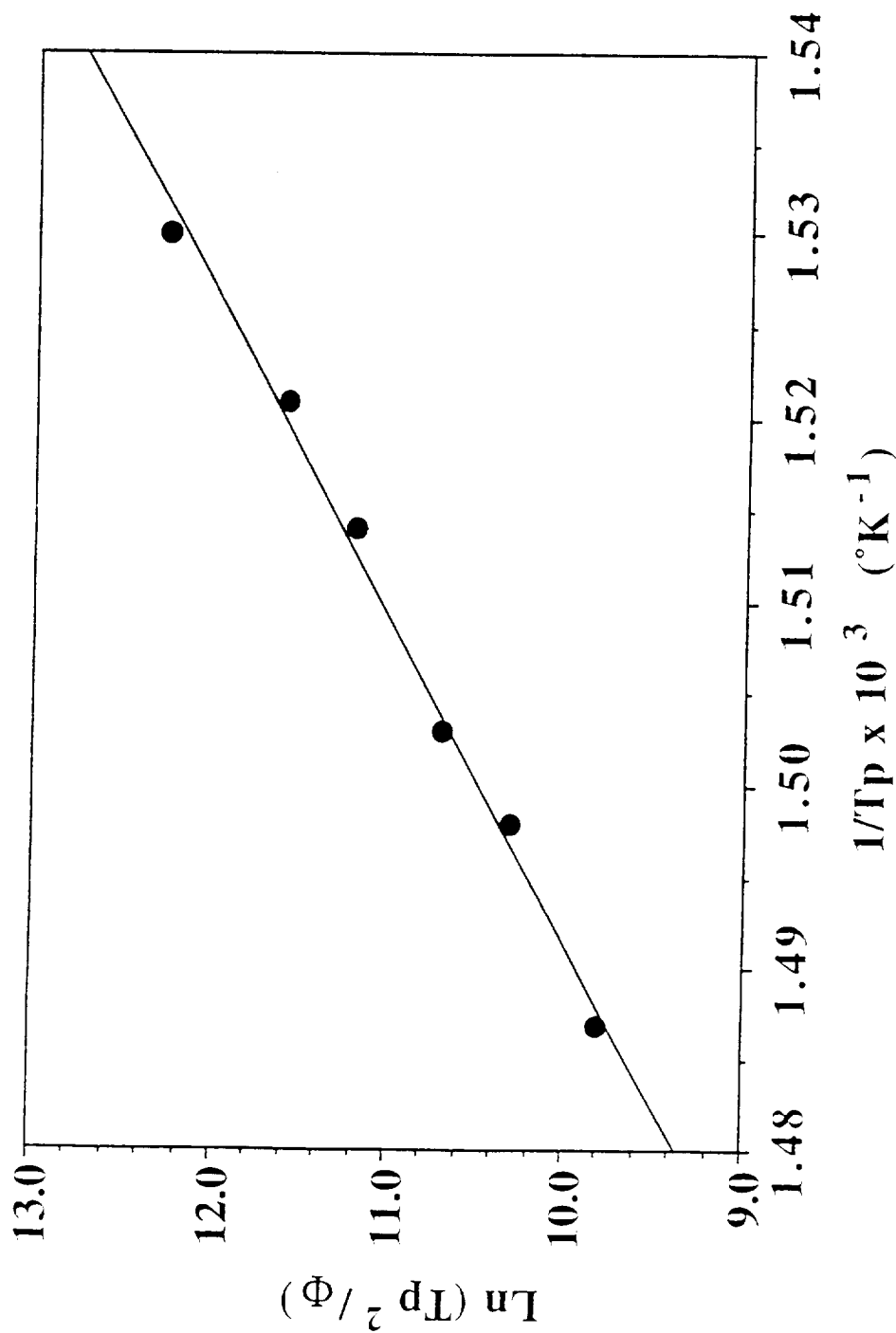
Fig. 4. The Kissinger plot for a 60PbO-10BiO$_{1.5}$-30GaO$_{1.5}$, cat%, glass (HMO-12, Table 2) where T_p is the temperature at the DTA crystallization peak maximum obtained at a heating rate of ϕ. The slope of this straight line yields an activation energy for crystallization of about 470 kJ/mol for this glass. Sample weight: 60 mg, Particle size: < 38 μm, Atmosphere: flowing nitrogen, $\phi = 2$, 4, 6, 10, 15 and 20° C/min.
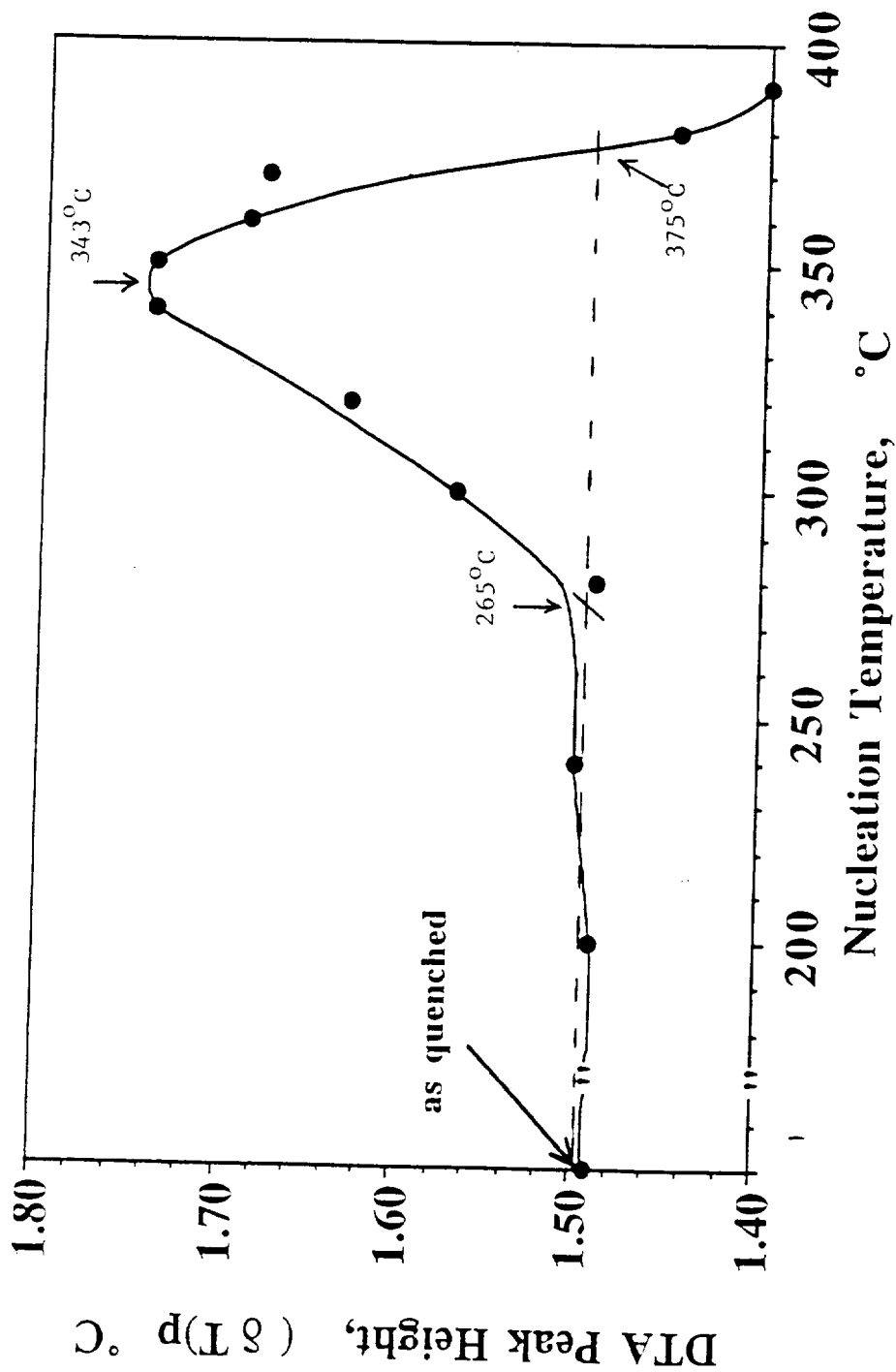
Fig. 5. Maximum intensity of the DTA crystallization peak, $(\delta T)_P$, for a 60PbO-10BiO$_{1.5}$-30GaO$_{1.5}$, cat%, glass (HMO-12, Table 2) as a function of nucleation temperature. Sample weight: 60 mg, Particle size: 180 to 300 μm, Nucleation time: 3 h, DTA heating rate: 15° C/min, Atmosphere: flowing nitrogen.
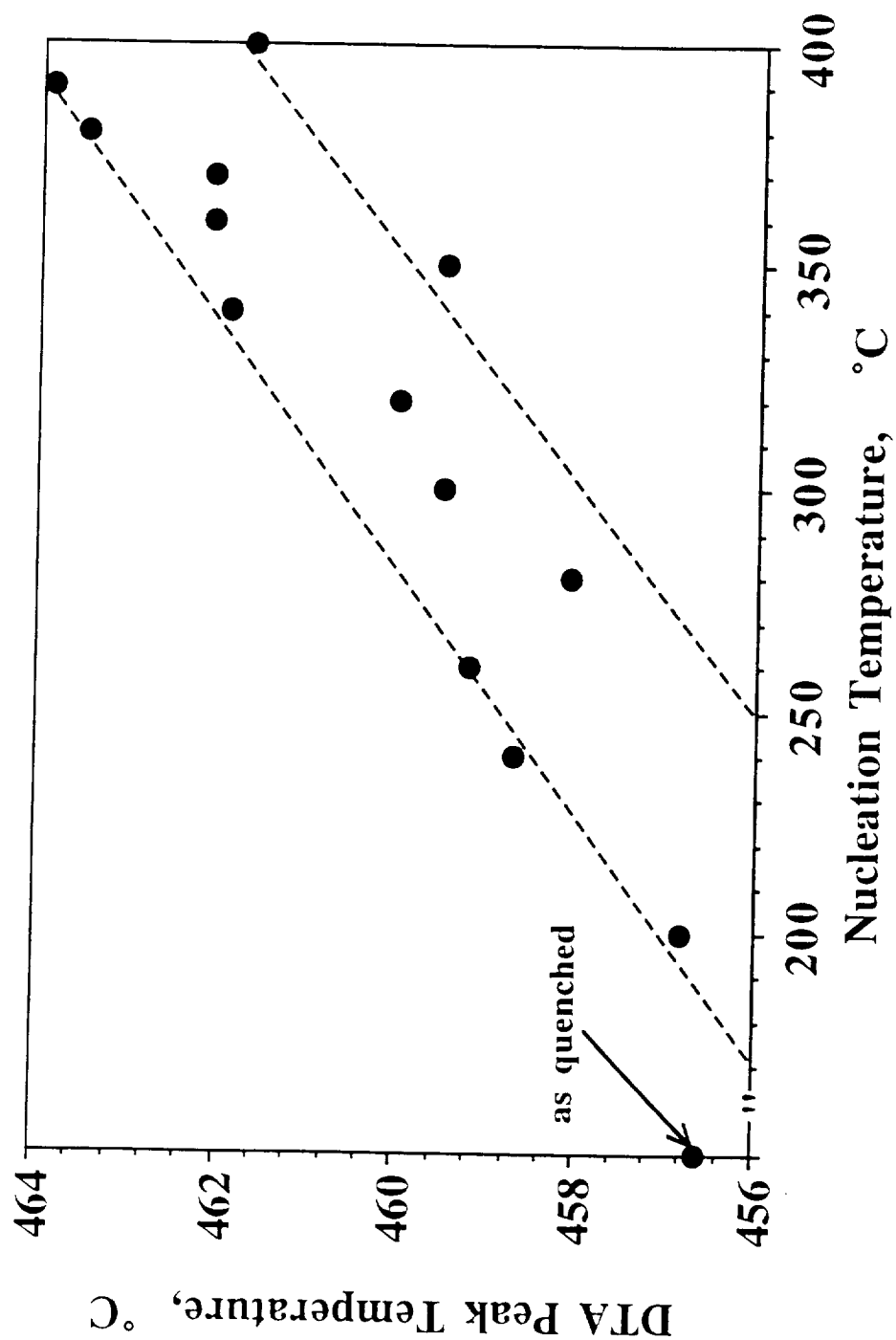
Fig. 6. Temperature at the DTA peak maximum for a 60PbO-10BiO$_{1.5}$-30GaO$_{1.5}$, cat%, glass (HMO-12, Table 2) as a function of nucleation temperature. For experimental conditions, see Fig. 5.
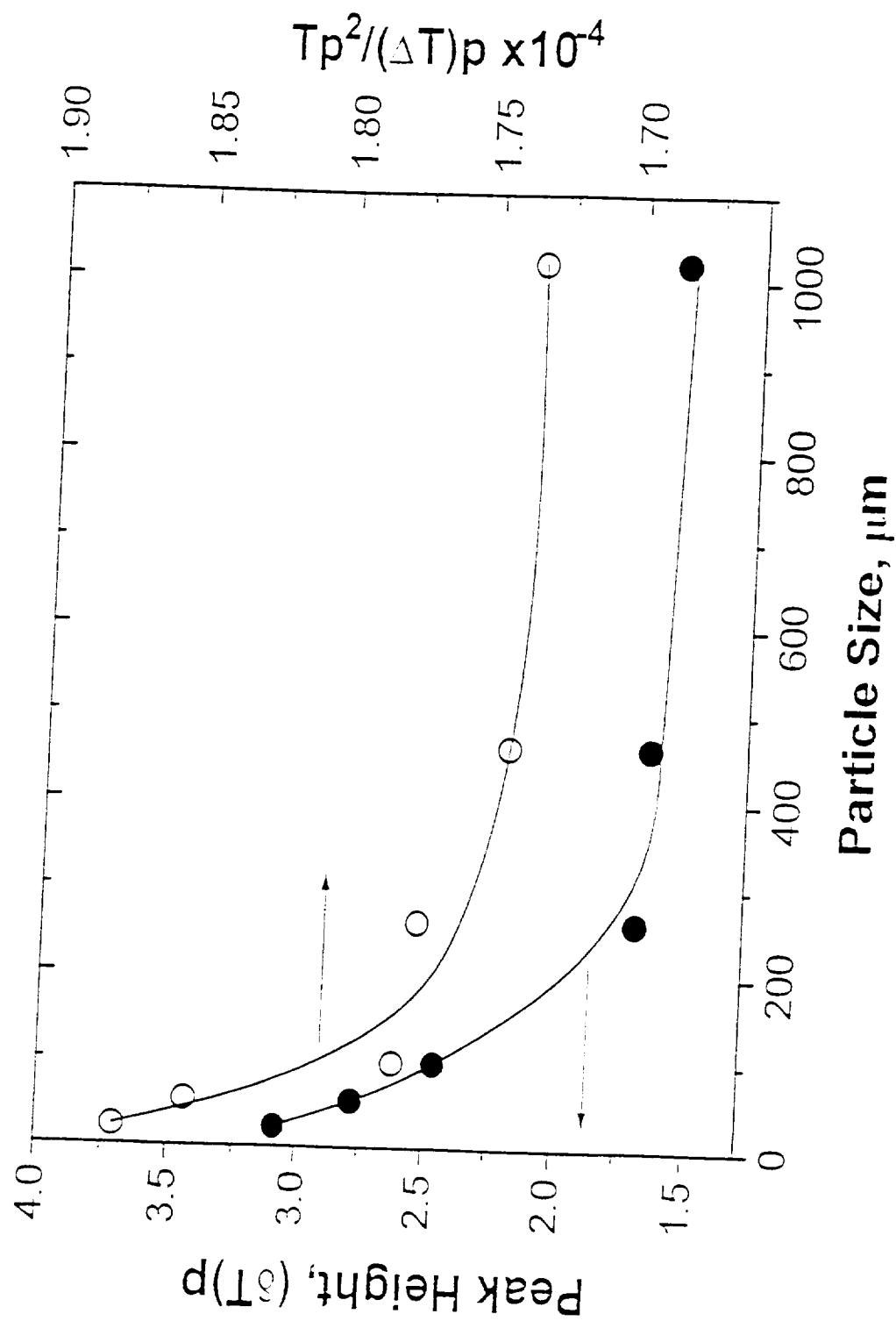
Fig. 7. DTA crystallization peak intensity, $(\delta T)_p$, and $T_p{}^2/(\Delta T)_p$, as a function of particle size for a $60PbO-10BiO_{1.5}-30GaO_{1.5}$, cat%, glass (HMO-12, Table 2), where $(\Delta T)_p$ is the peak half width and T_p is the temperature at the DTA peak maximum. Sample weight: 40 mg, Atmosphere: flowing nitrogen, DTA heating rate: 15° C/min.
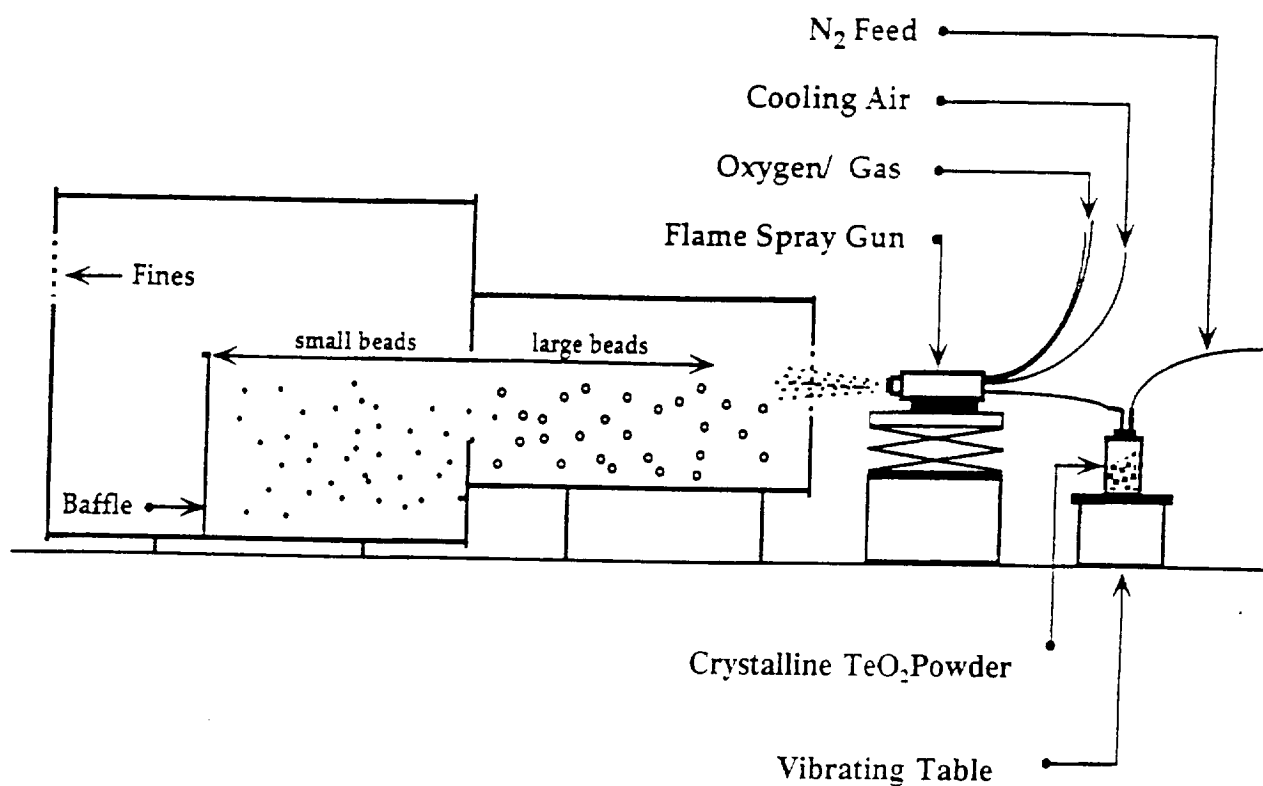
Fig. 8. Schematic of the apparatus used to prepare TeO_2 glass microspheres. Powder of crystalline TeO_2 raw material is fed through oxygen-propane flame. The microspheres are collected in stainless steel barrels.

Labels in figure: N₂ Feed, Cooling Air, Oxygen/ Gas, Flame Spray Gun, Fines, small beads, large beads, Baffle, Crystalline TeO₂Powder, Vibrating Table
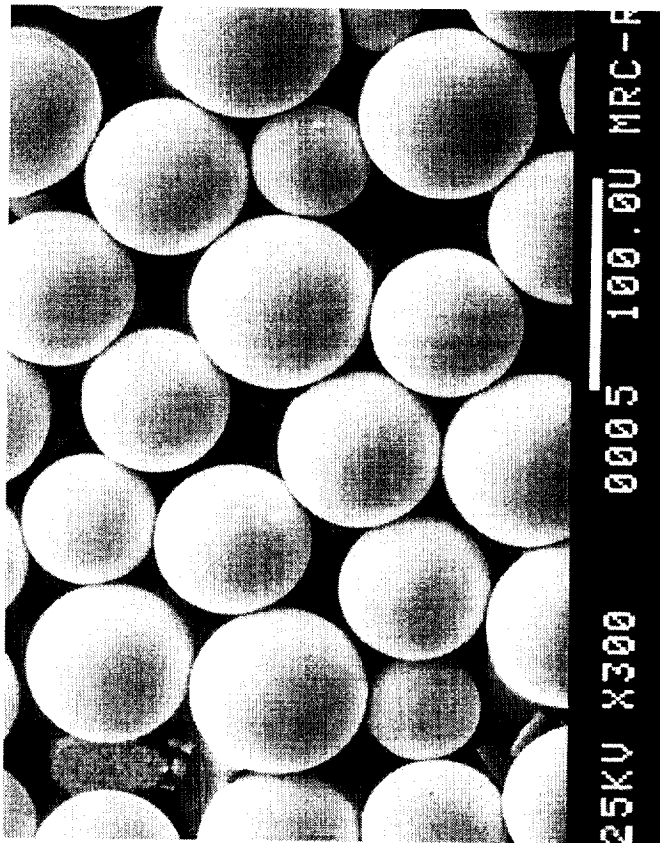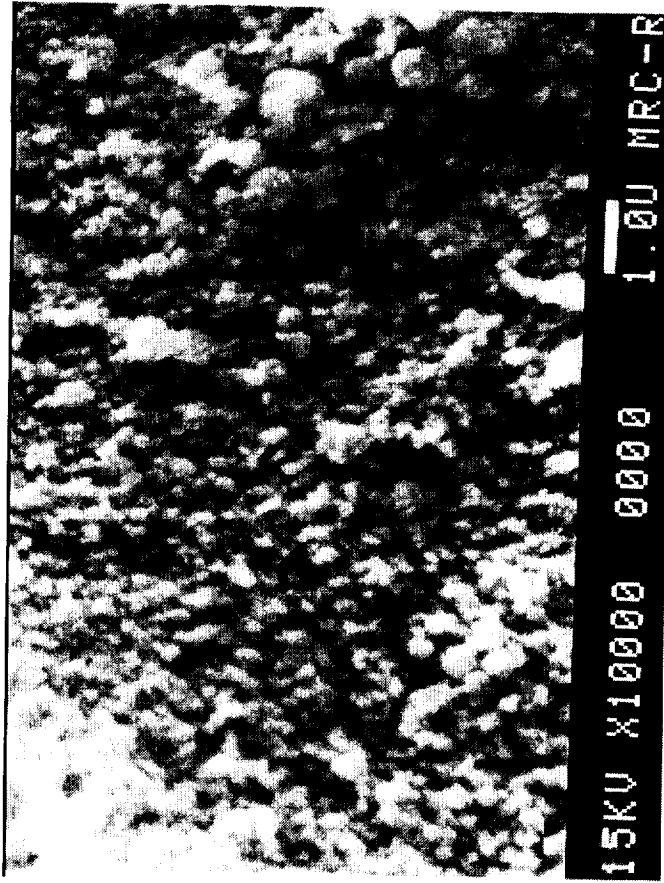
Fig. 9. SEM photograph of the glass microspheres prepared from crystalline TeO_2 powder by (A) flame fusion (FS beads) and (B) vapor deposition (VD beads). While (FS beads) have a diameter ranging from 50 to 75 µm, the diameter of the (VD beads) is typically < 1 µm.

49
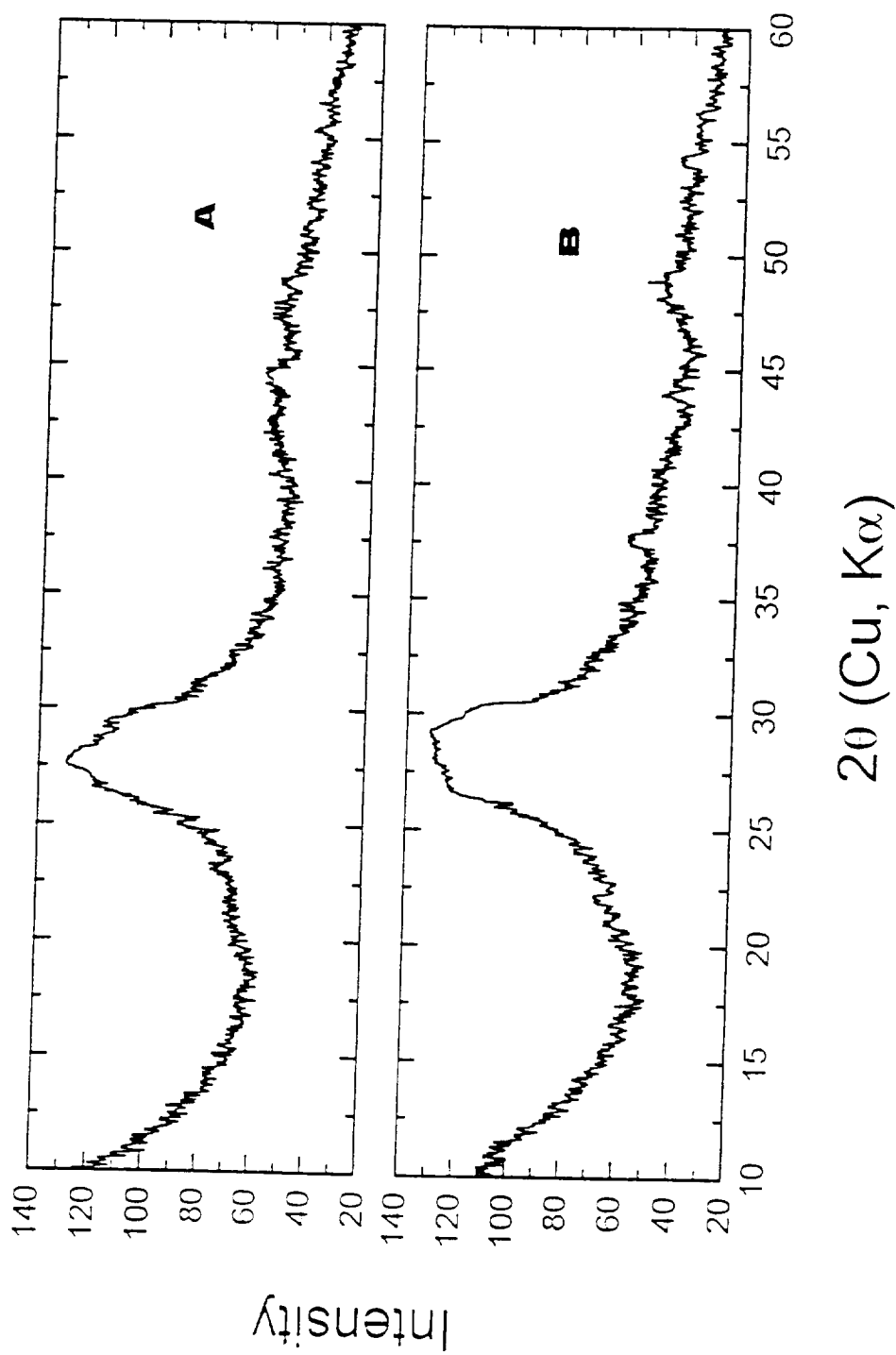
Fig. 10. X-ray diffraction analysis (XRD) of the microspheres shown in Fig. 9 prepared from crystalline TeO_2 powder by (A) vapor deposition (VD beads) and (B) flame fusion (FS beads). As analyzed by XRD, both types of beads are essentially amorphous.

50
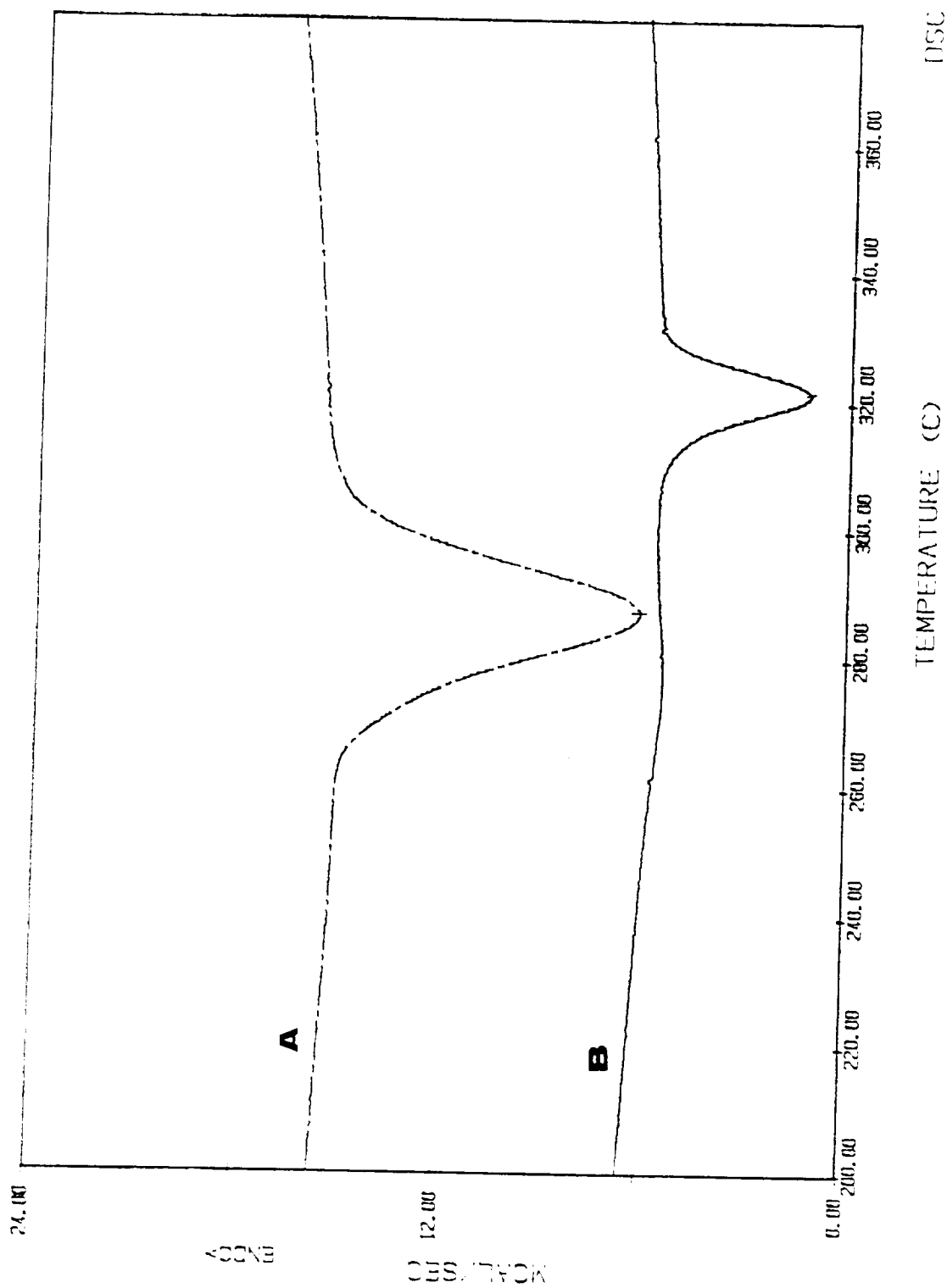
Fig. 11. DSC thermograms for the glass microspheres prepared by (A) flame fusion (FS beads) and (B) vapor deposition (VD beads) from crystalline TeO_2 powder. The weight and DSC heating rate were constant at about 8.9 mg and 10° C/min, respectively, for both samples. The crystallization temperature is higher and the DSC peak area is smaller for the VD beads than those for the FS beads, which indicates that the VD beads are more resistant to crystallization than the FS beads.
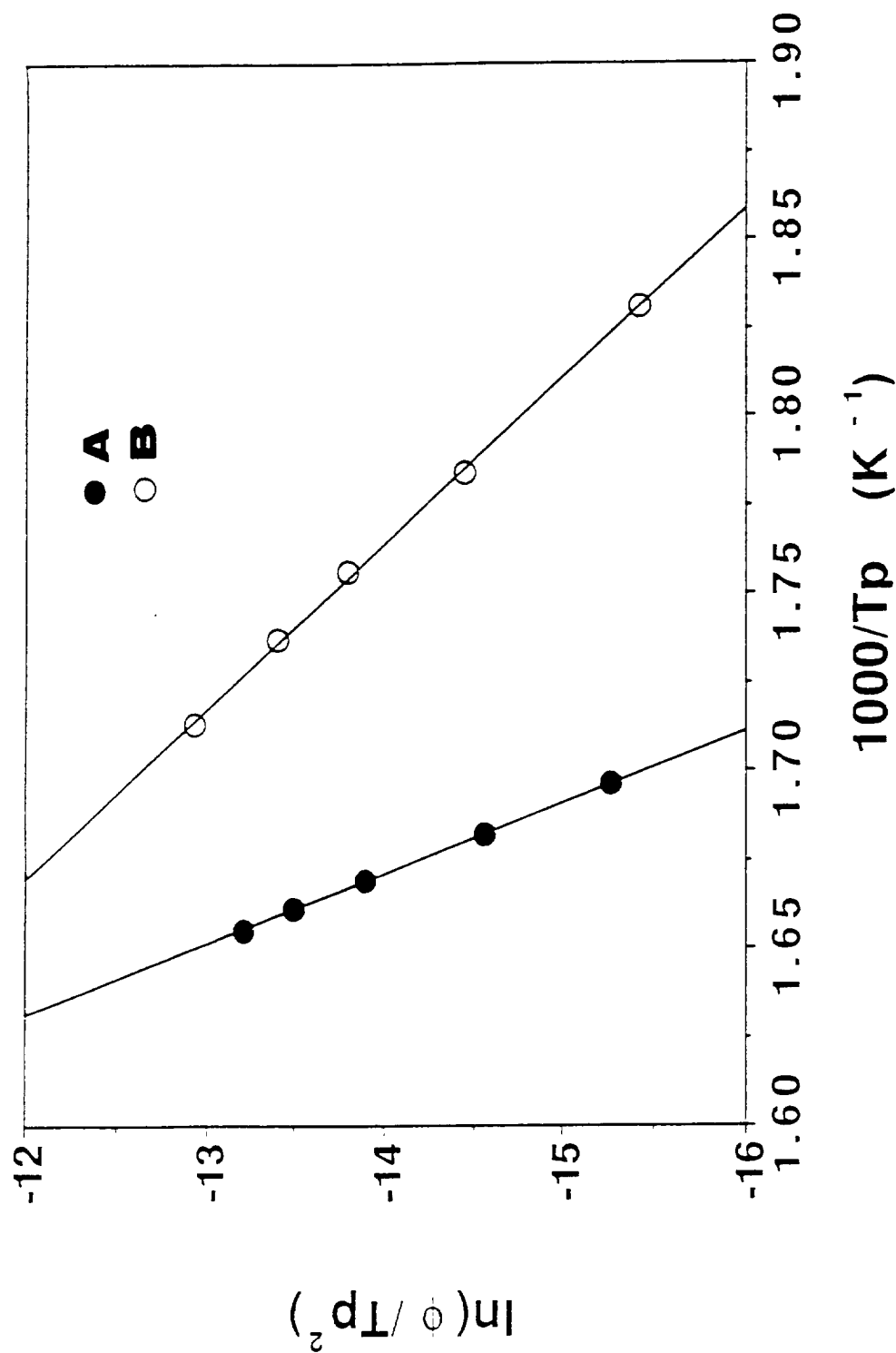
Fig. 12. Kissinger plots for the glass microspheres prepared from crystalline TeO_2 powder by (A) vapor deposition (VD beads) and (B) flame fusion (FS beads). T_p is the temperature at the DSC peak maximum obtained at heating rates (ϕ) of 5, 10, 20, 30 and 40° C/min. The slope of these straight lines yielded the activation energy for crystallization of about 172 and 418 kJ/mol for the FS beads and VD beads, respectively.
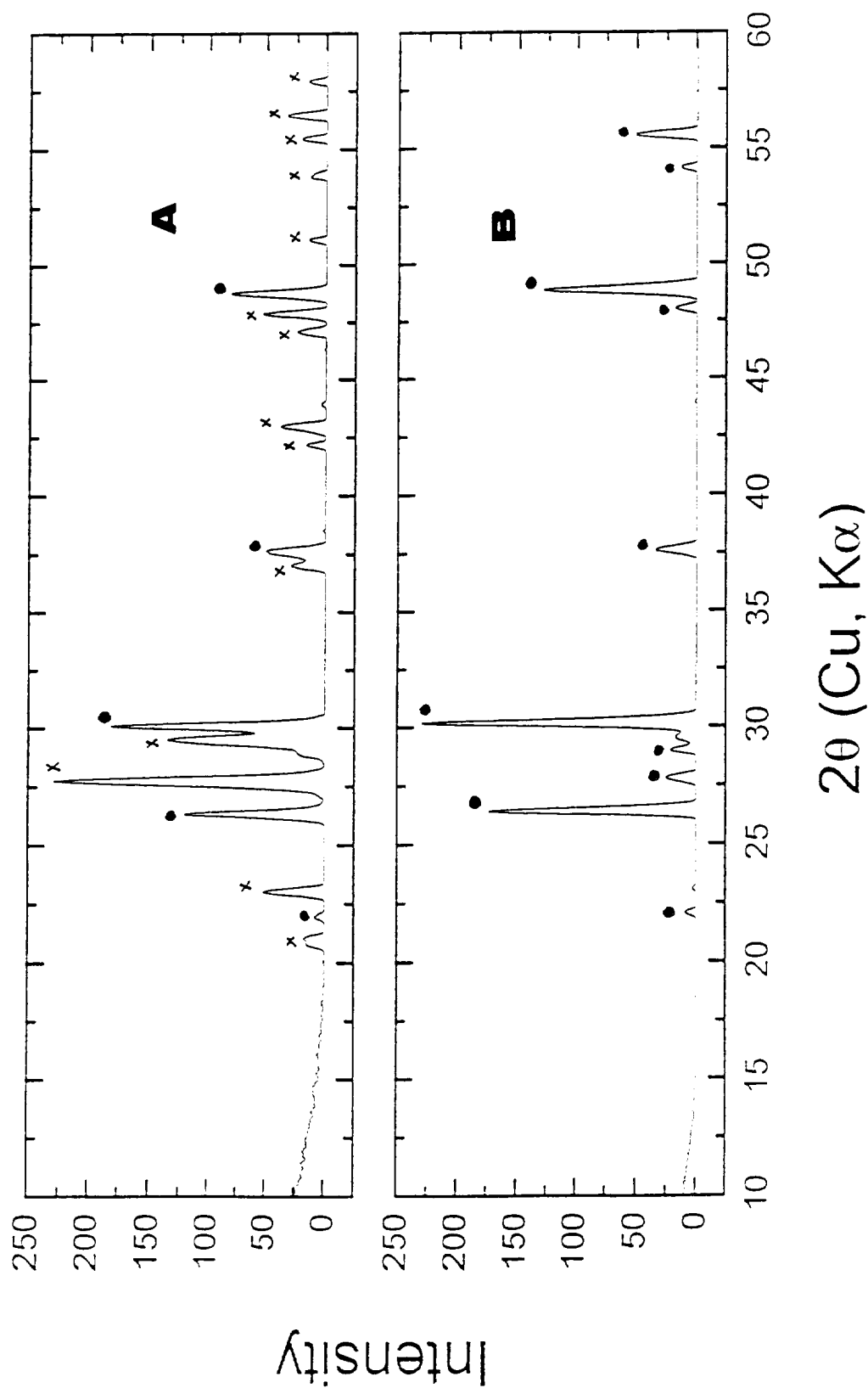
Fig. 13. X-ray diffraction analysis (XRD) of the crystallized glass microspheres prepared from crystalline TeO_2 powder by (A) vapor deposition (VD beads) and (B) flame fusion (FS beads). XRD peaks for the crystallized FS beads were identified as those of α-TeO_2. The peaks for the crystallized VD beads may contain a few peaks of α-TeO_2, but a majority of the peaks could not be identified. ●: α-TeO_2,   x: unknown

53
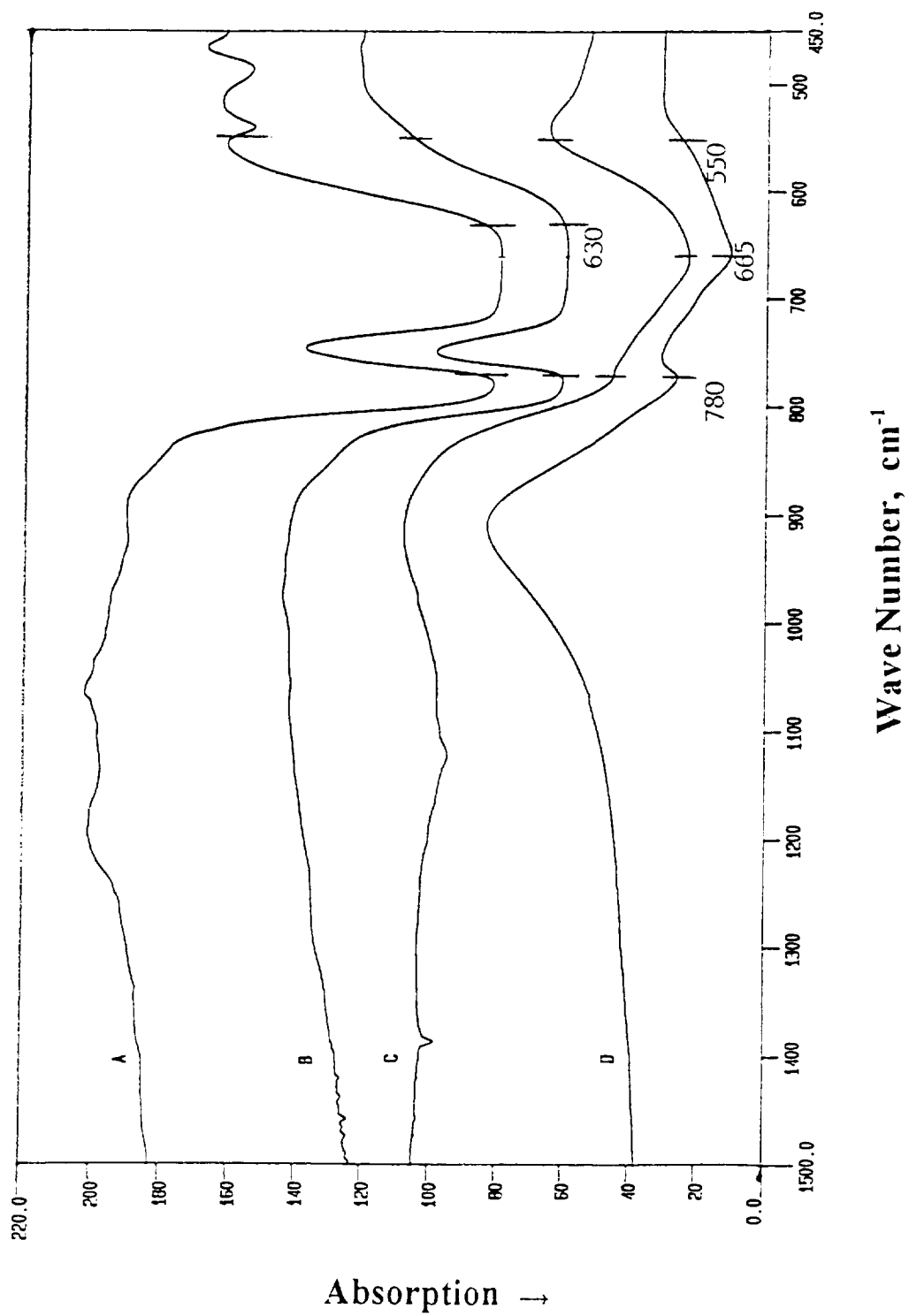
Fig. 14. IR spectra of the glassy and crystalline microspheres prepared from crystalline TeO_2 powder by flame fusion (FS beads) and vapor deposition (VD beads). A: crystalline VD beads, B: crystalline FS beads, C: glassy VD beads, D: glassy FS beads.

54
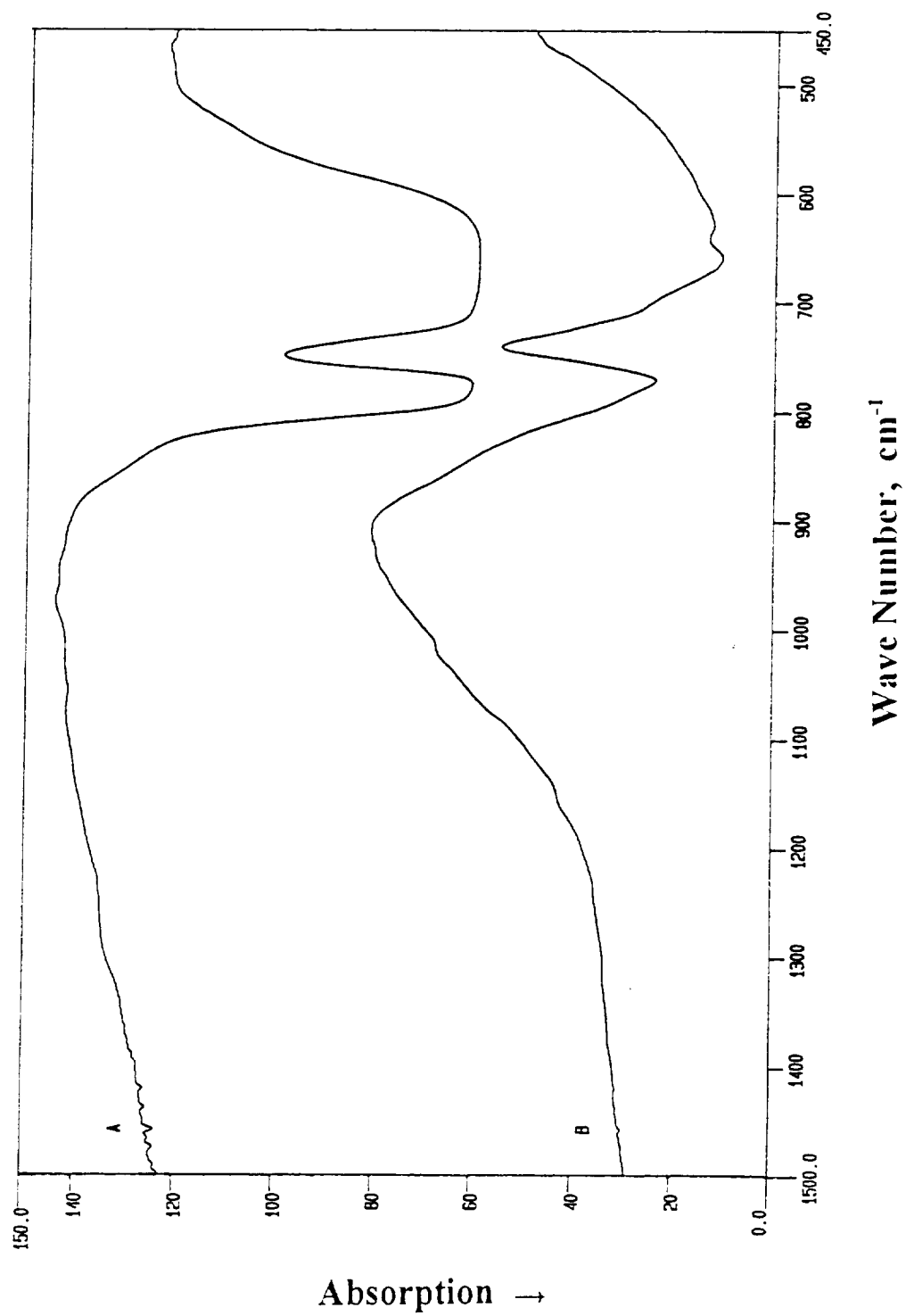
Fig. 15. IR spectra for the (A) crystalline FS beads and (B) TeO_2 raw material. See Fig. 14 also.
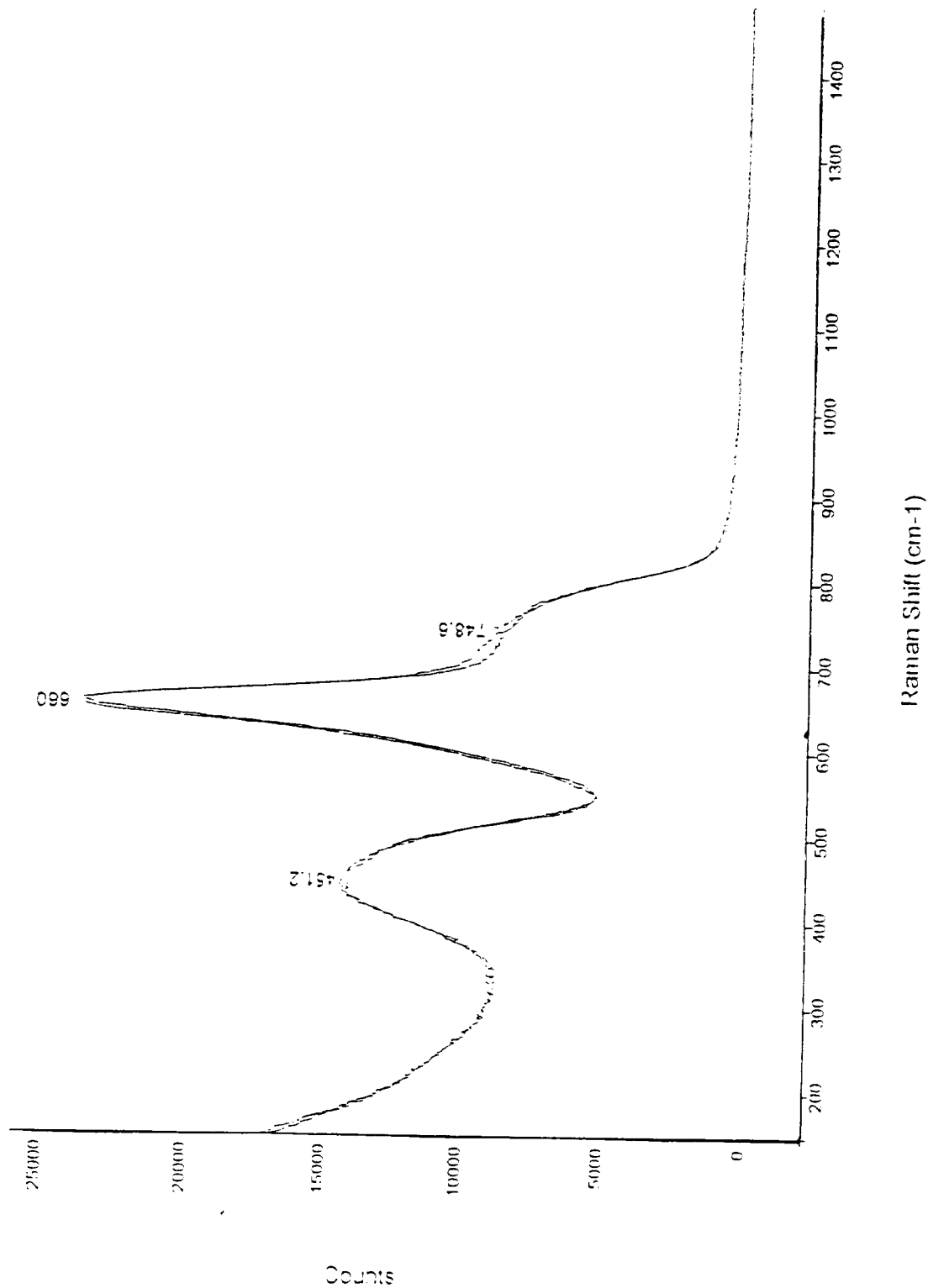
Fig. 16. Raman spectra for the glass beads prepared from crystalline TeO$_2$ powder by flame fusion (FS beads), and vapor deposition (VD beads). The Raman spectra for these two types of beads are indistinguishable.
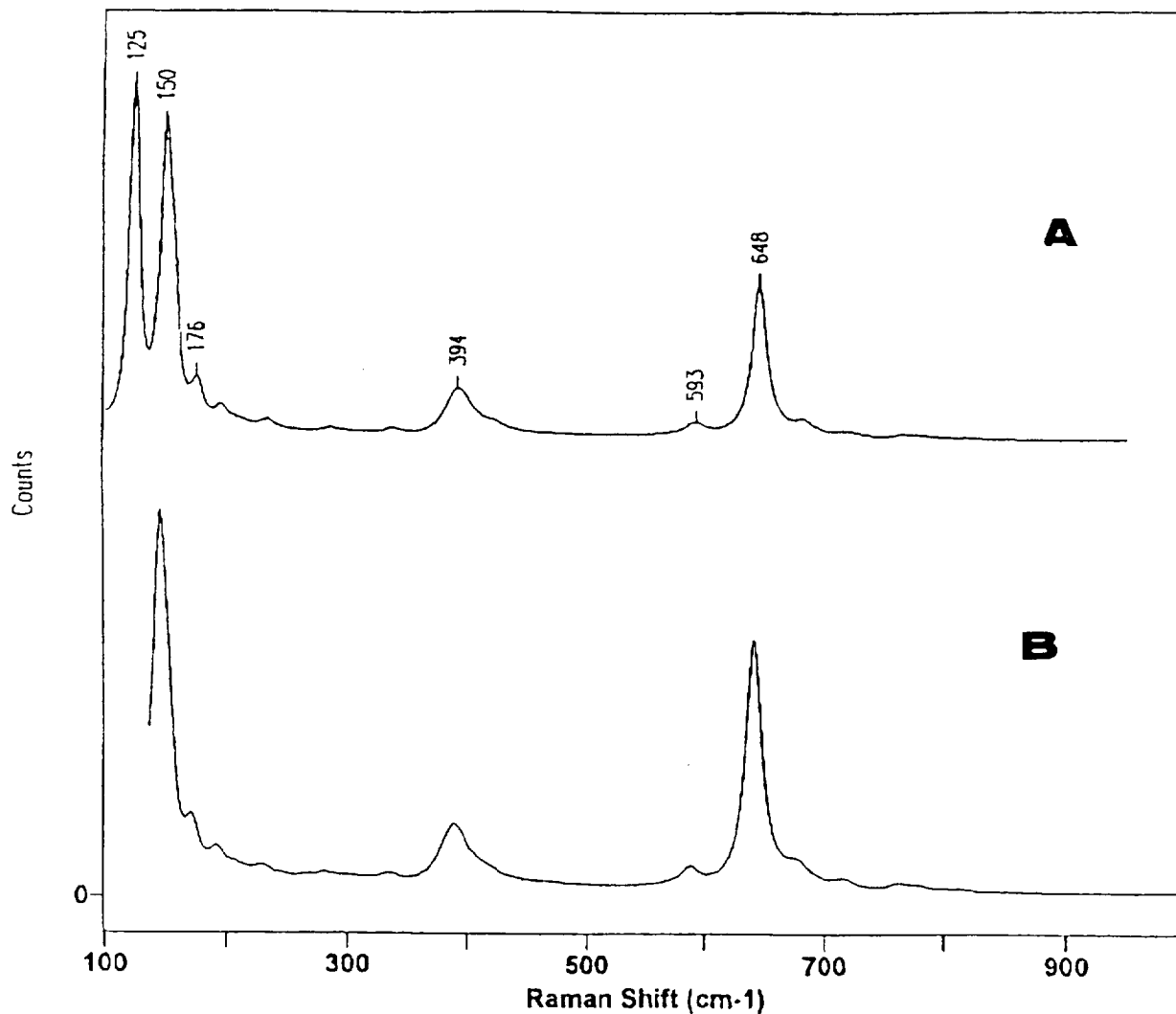
Fig. 17. Raman spectra for the crystalline (A) FS beads and (B) VD beads. The beads were crystallized at 300° C for 3 h. The peaks are identified primarily as those of α-TeO₂ (paratellurite). For Raman spectra of the glassy FS and VD beads, see Fig. 16.
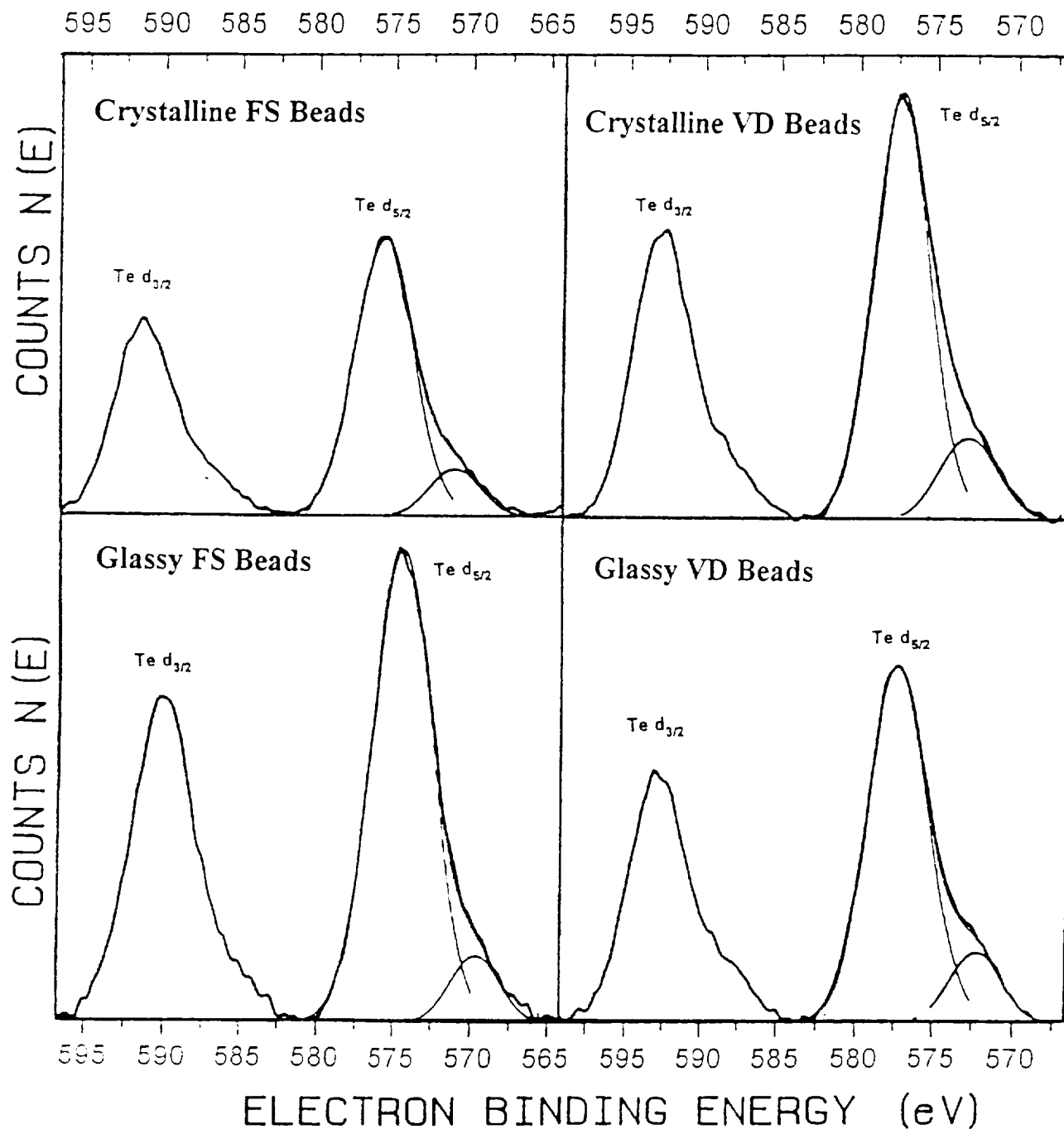
Fig. 18. X-ray photoelectron spectra (XPS) for the glassy and crystalline microspheres prepared from crystalline TeO_2 powder by flame fusion (FS beads) and vapor deposition (VD beads). The glass beads were crystallized at 300° C for 3 h. See Table 3 for Te $d_{5/2}$ binding energy for different samples.
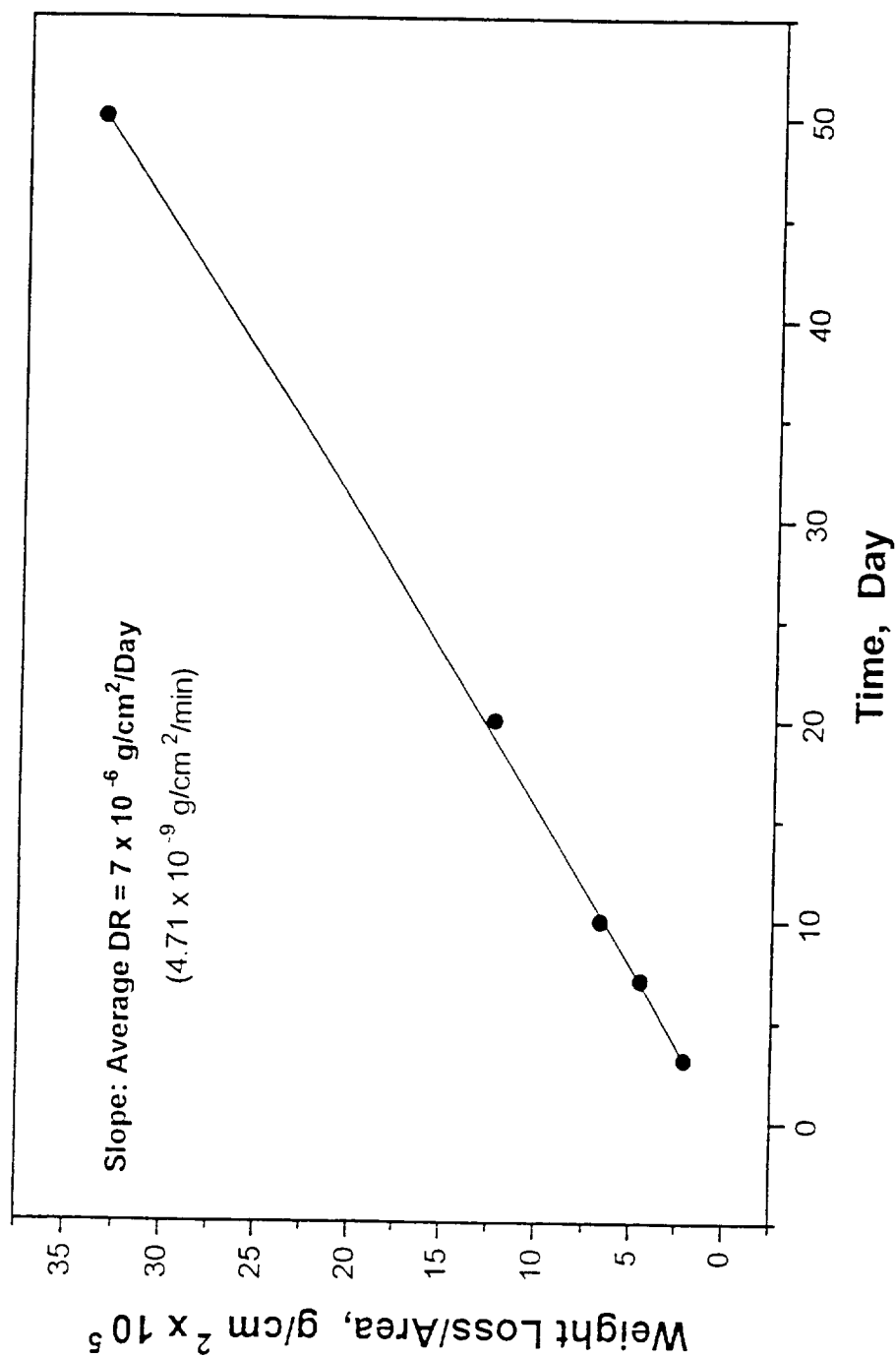
Fig. 19. Weight loss per cm^2 as a function of time in deionized water at room temperature for the glass beads prepared from crystalline TeO$_2$ powder by flame fusion (FS beads).
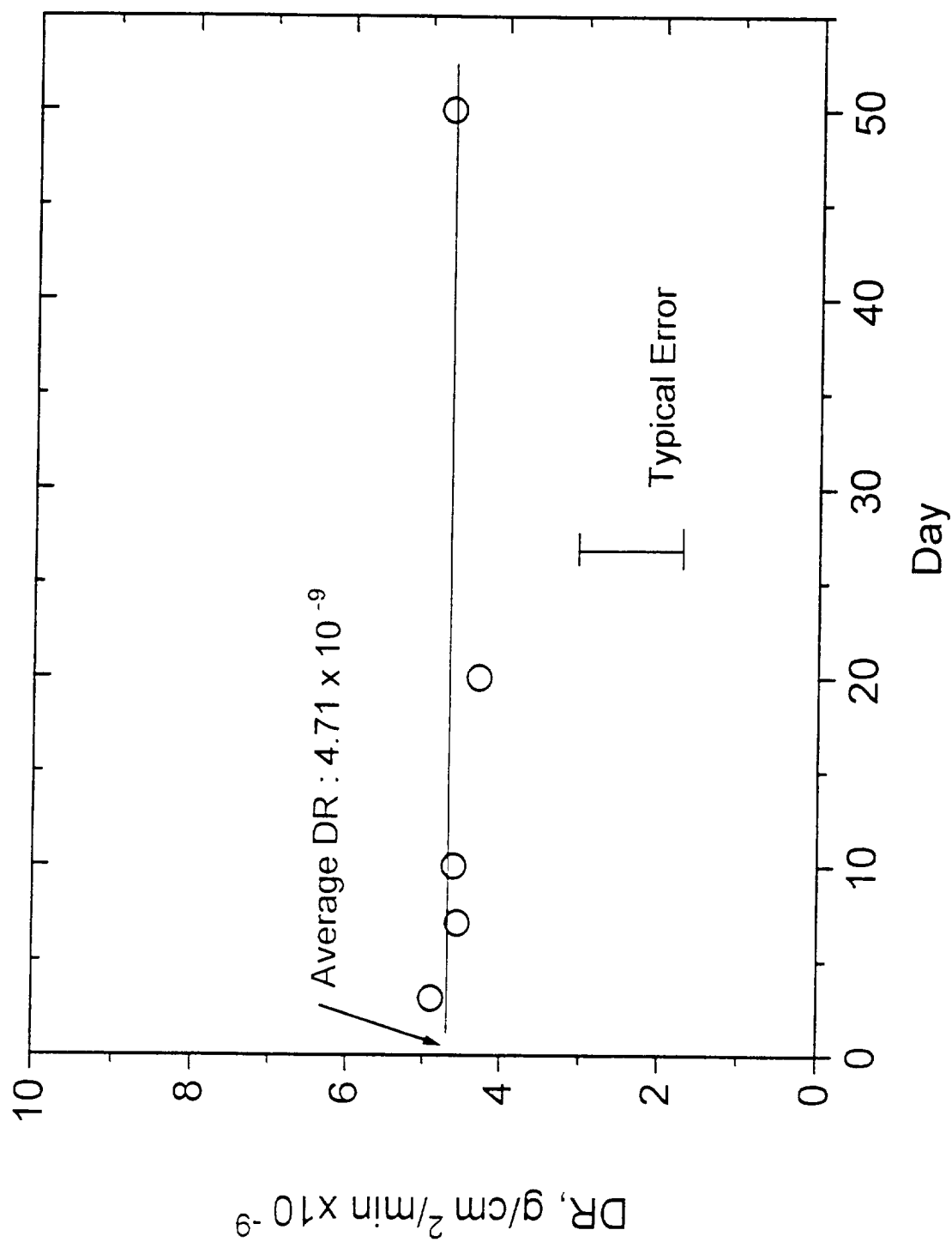
Fig. 20. Dissolution rate, DR, in deionized water at different times (open circles) for the glass beads prepared from crystalline TeO_2 powder by flame fusion (FS beads). The average DR determined from the slope of the straight line in Fig. 19 is also included (solid line).
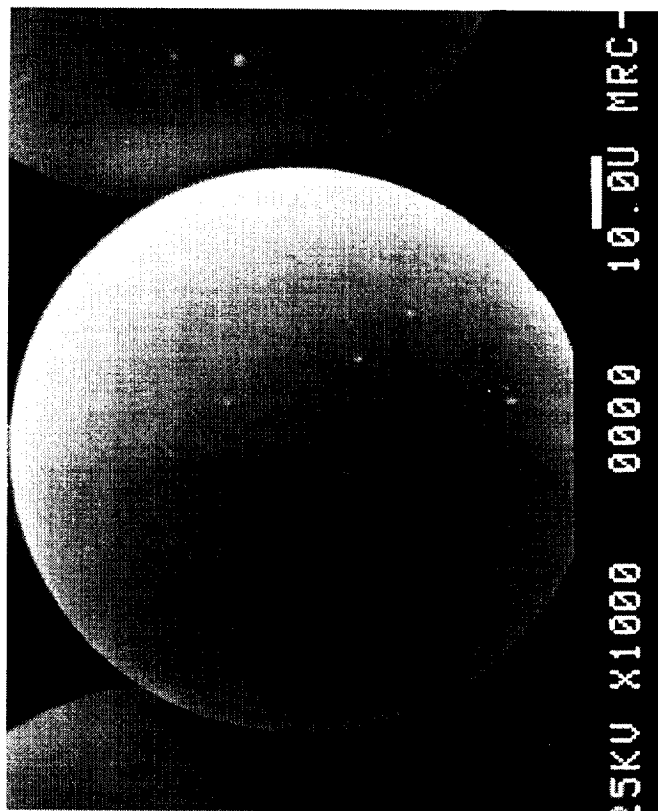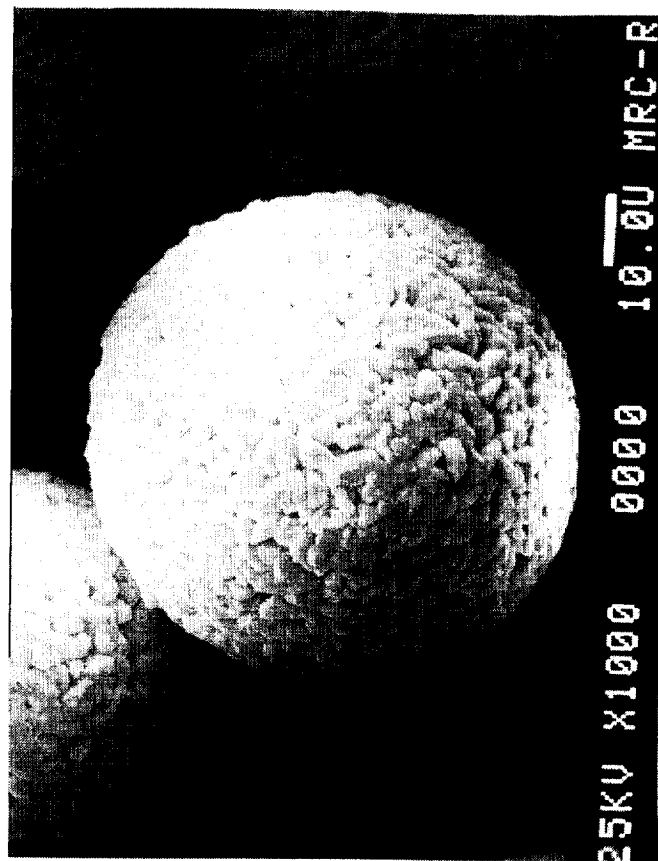
Fig. 21. TeO₂ glass microspheres prepared by flame synthesis method (FS beads) after (A) exposing them to ambient atmosphere for 7 days and (b) immersing them in deionized water for 2 days. Severe surface degradation of the glass beads are observed (Fig. B) when treated in water, but the beads appears to remain chemically durable in ambient atmosphere at least for 7 days (Fig. A).
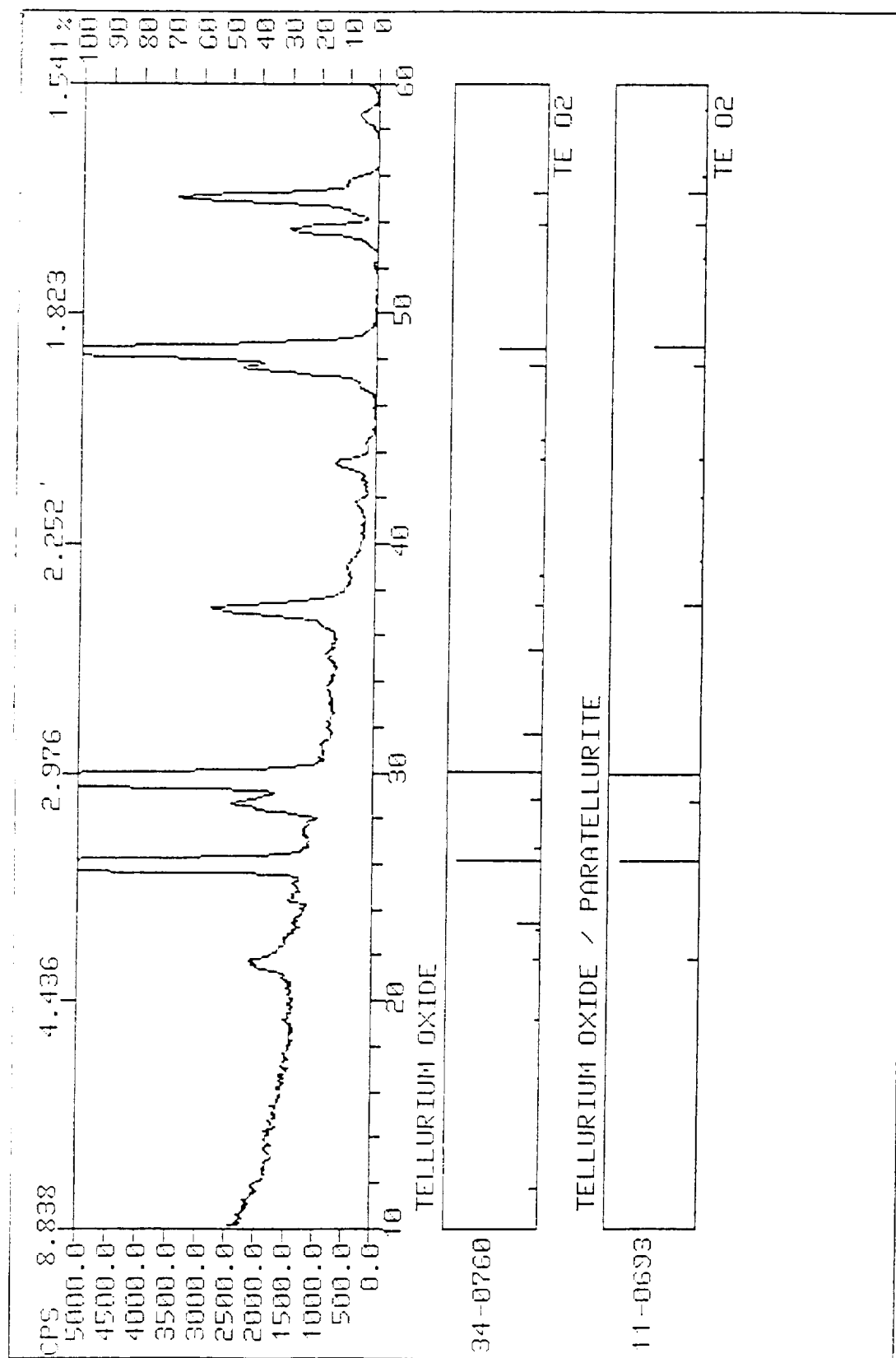
Fig. 22. XRD of the FS glass beads (prepared by flame fusion of crystalline TeO_2 powder) after immersing them in deionized water for 2 days. The peaks are essentially identical to those of α-TeO_2 (paratellurite). For surface morphology of these water treated beads, see Fig. 21B.

62
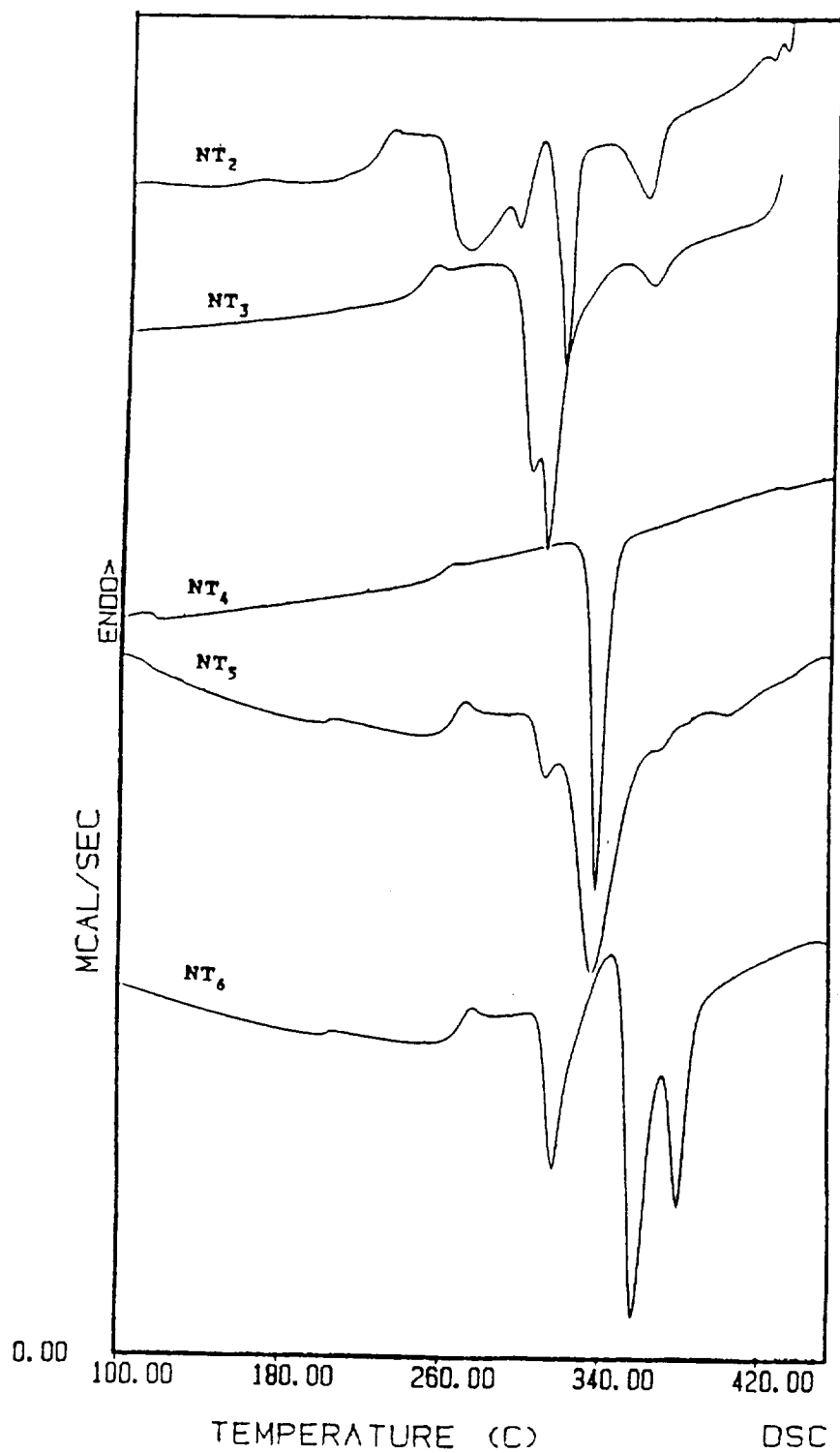
Fig. 23. DSC curves for the sodium tellurite glasses NT_x ($Na_2O.xTeO_2$) where x = 2, 3, 4, 5 and 6. Sample weight: 20 mg, Sample pan: aluminum, DSC heating rate: $10°$ C/min, Atmosphere: flowing nitrogen.
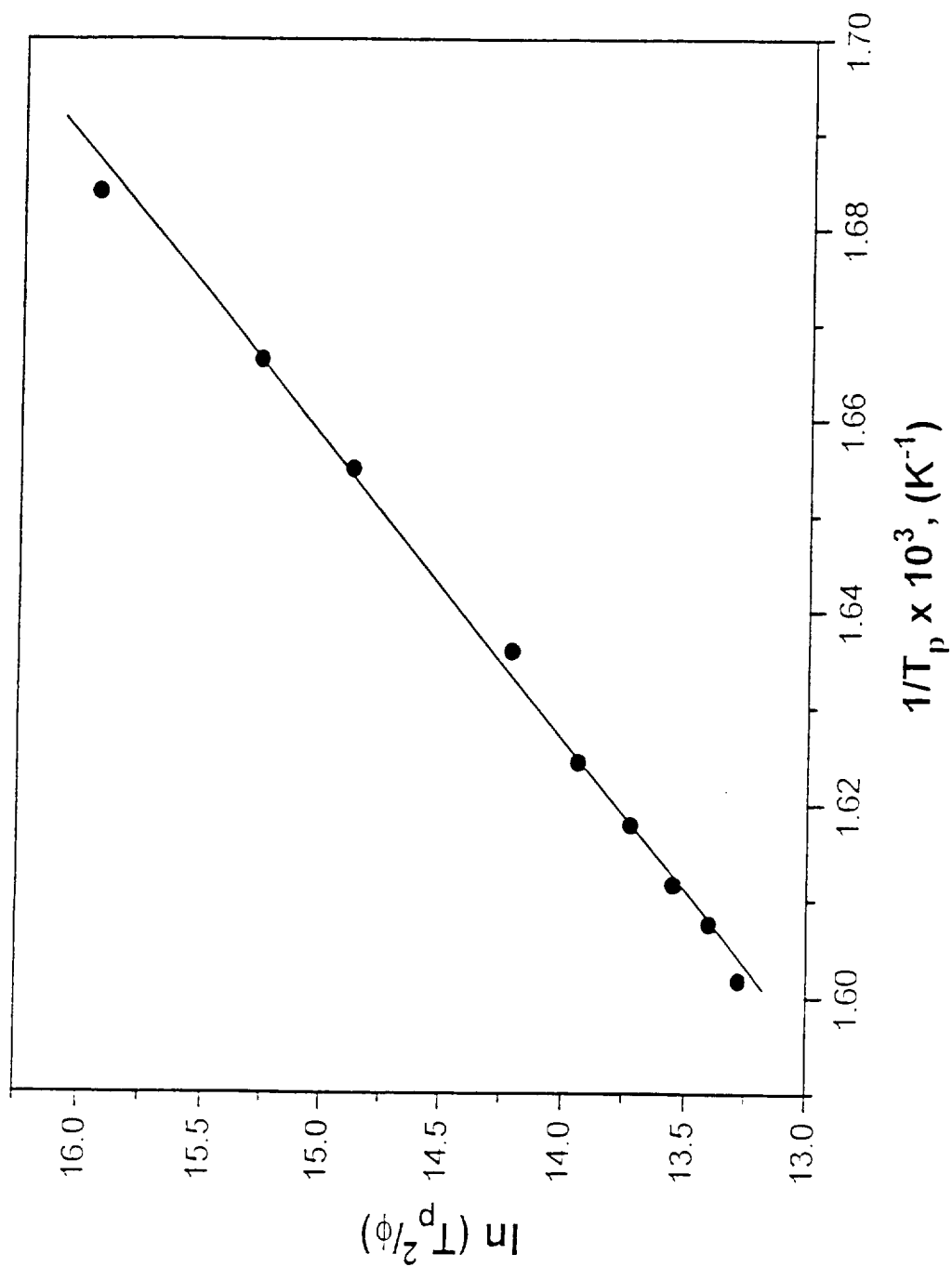
Fig. 24. Kissinger plot for the $Na_2O.4TeO_2$ (NT_4) glass obtained from DSC measurements at heating rates (ϕ) of 2.5, 5, 7.5, 15, 20, 25, 30, 35 and 40° C/min. T_p is the temperature at the DSC peak maximum. Sample weight: 26±1 mg, Particle size: 35 to 45 μm.
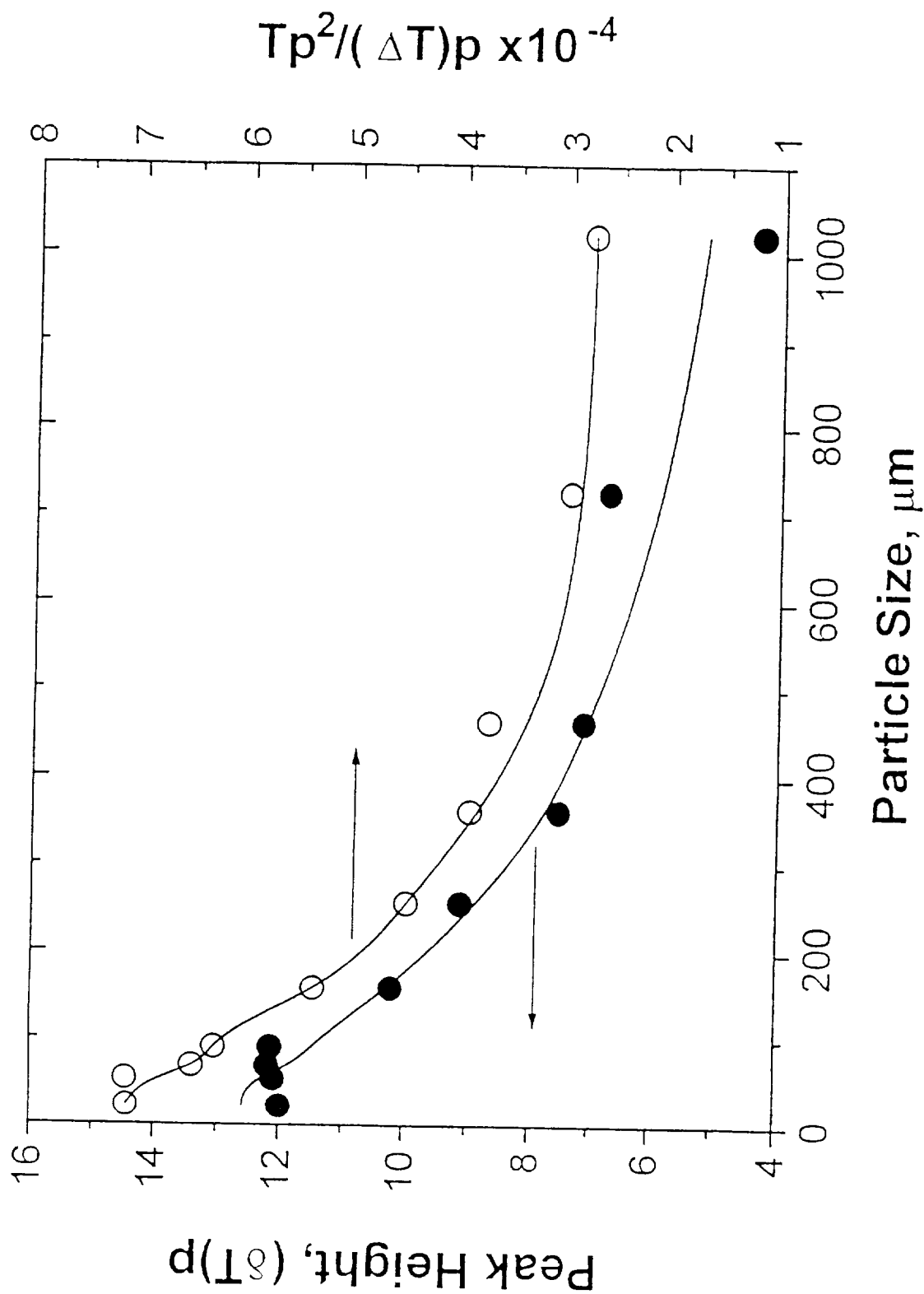
Fig. 25. DTA crystallization peak intensity, $(\delta T)_p$, and $T_p^2/(\Delta T)_p$, as a function of particle size for a $20Na_2O-80TeO_2$, mol%, glass (NT_4), where $(\Delta T)_p$ is the peak half width and T_p is the temperature at the DTA peak maximum. Sample weight: 40 mg, Atmosphere: flowing nitrogen, DTA heating rate: 15° C/min.
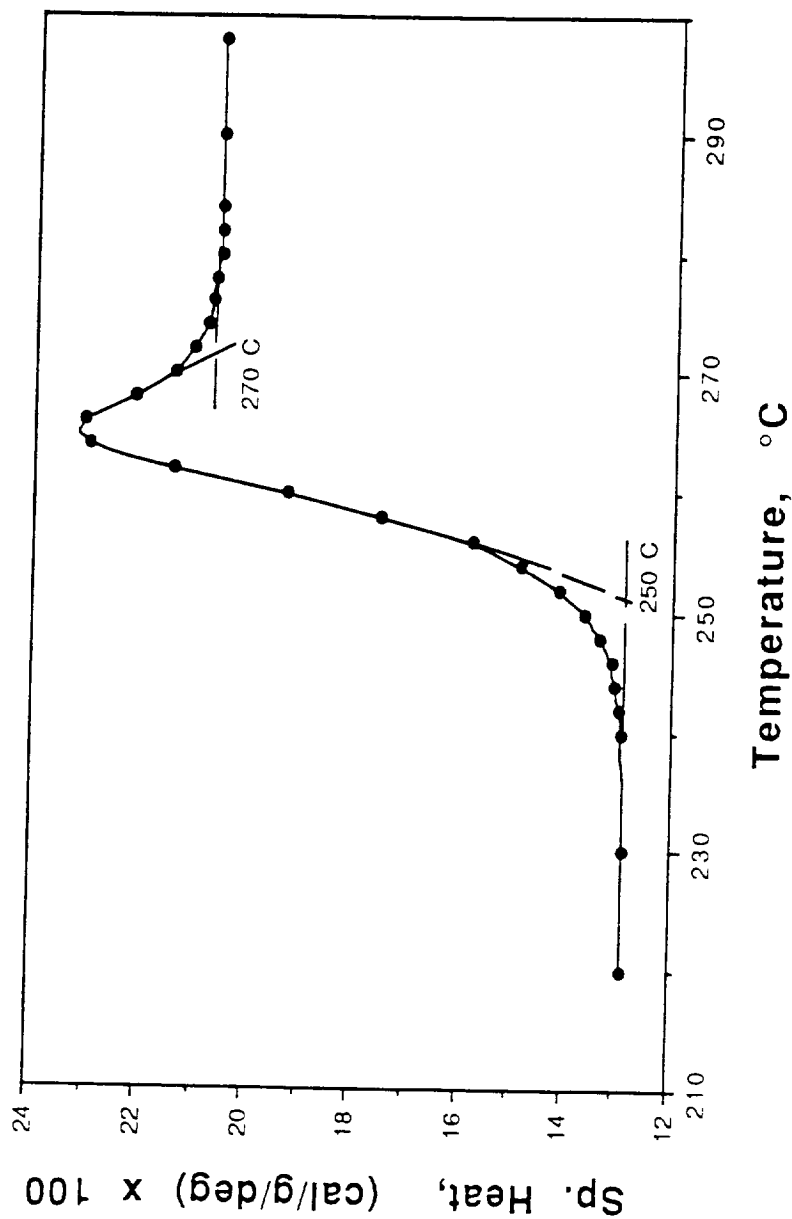
Fig. 26. Specific heat (c_p) versus temperature plot for an $Na_2O.4TeO_2$ (NT_4) glass at a heating rate of 20° C/min. Particle size of the sample: 425 to 500 μm.
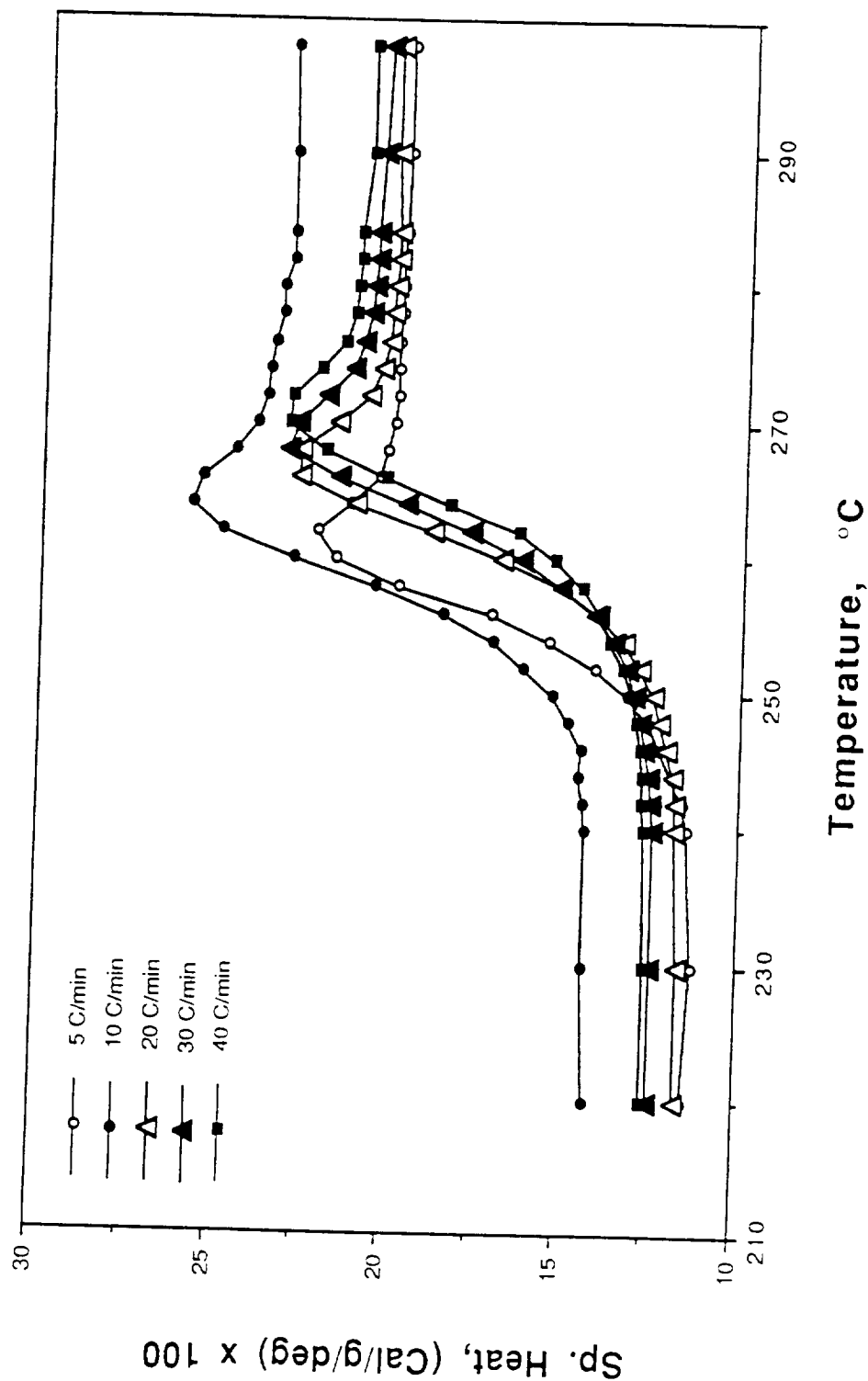
Fig. 27. Specific heat (c_p) versus temperature plots for an $Na_2O.4TeO_2$ (NT_4) glass at different heating rates shown. Sample particle size: 120 to 166 μm. Although, T_{g1} (lower temperature of the glass transition region) was close, T_{g2} (upper temperature of the glass transition region) increased considerably with increasing heating rate, see also Table 5.
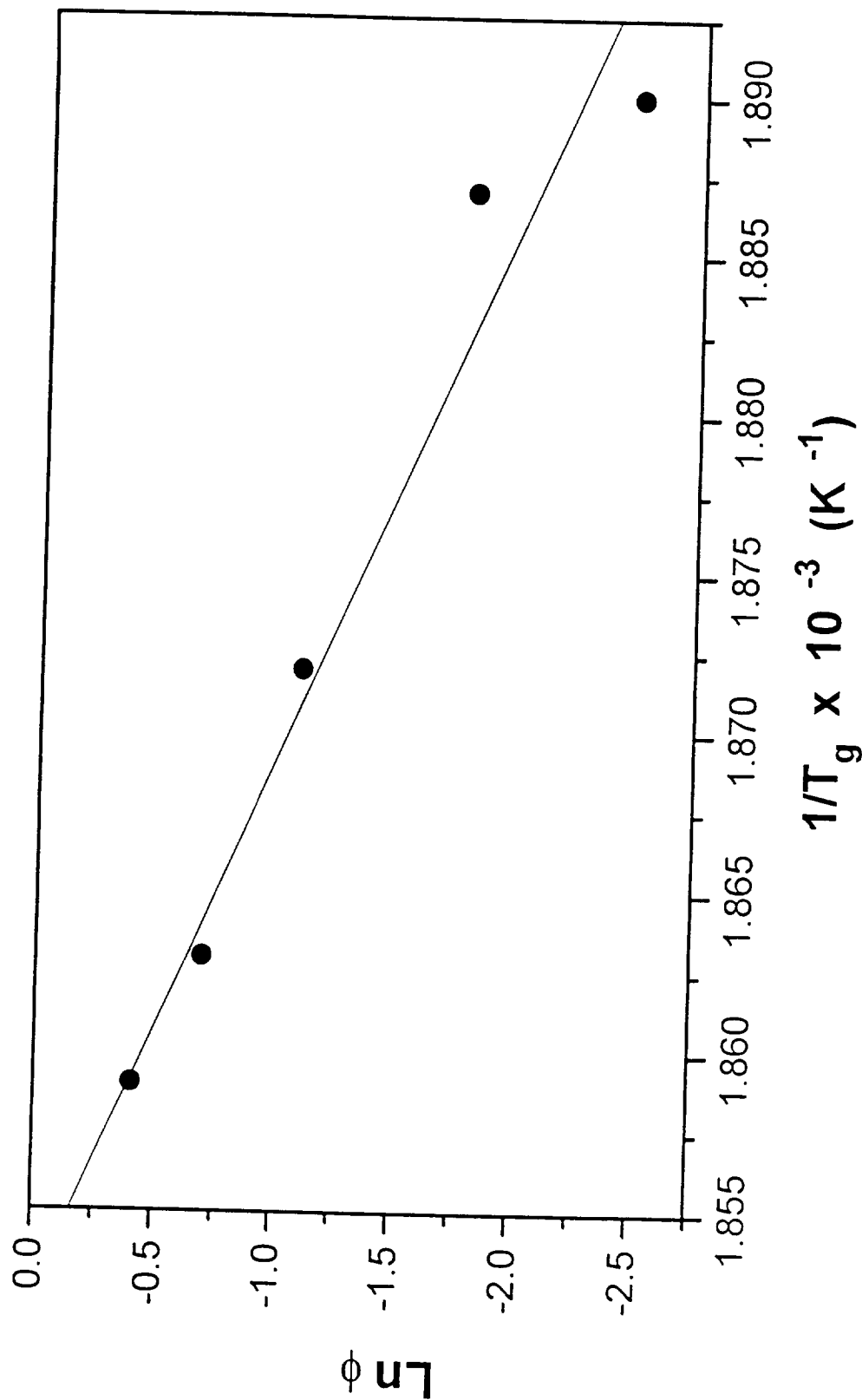
Fig. 28. Plot of $Ln\phi$ vs $1/T_g$ for an $Na_2O.4TeO_2$ (NT_4) glass where T_g is the average glass transition temperature obtained at a heating rate of ϕ. The slope of this straight line yields an activation energy for glass transition of about 530 kJ/mol.
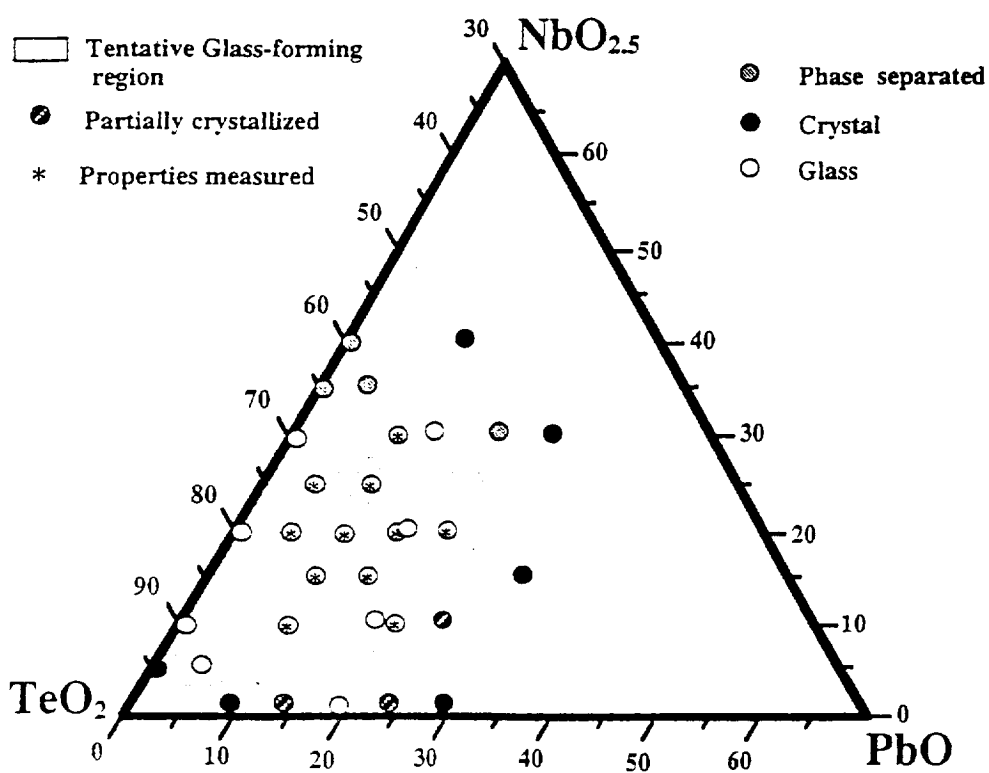
Fig. 29. Glass forming region as determined by melting a 10 g batch and casting the melt on to a steel plate for the PbO-NbO$_{2.5}$-TeO$_2$ compositions. Glasses for which the properties were measured are also shown.
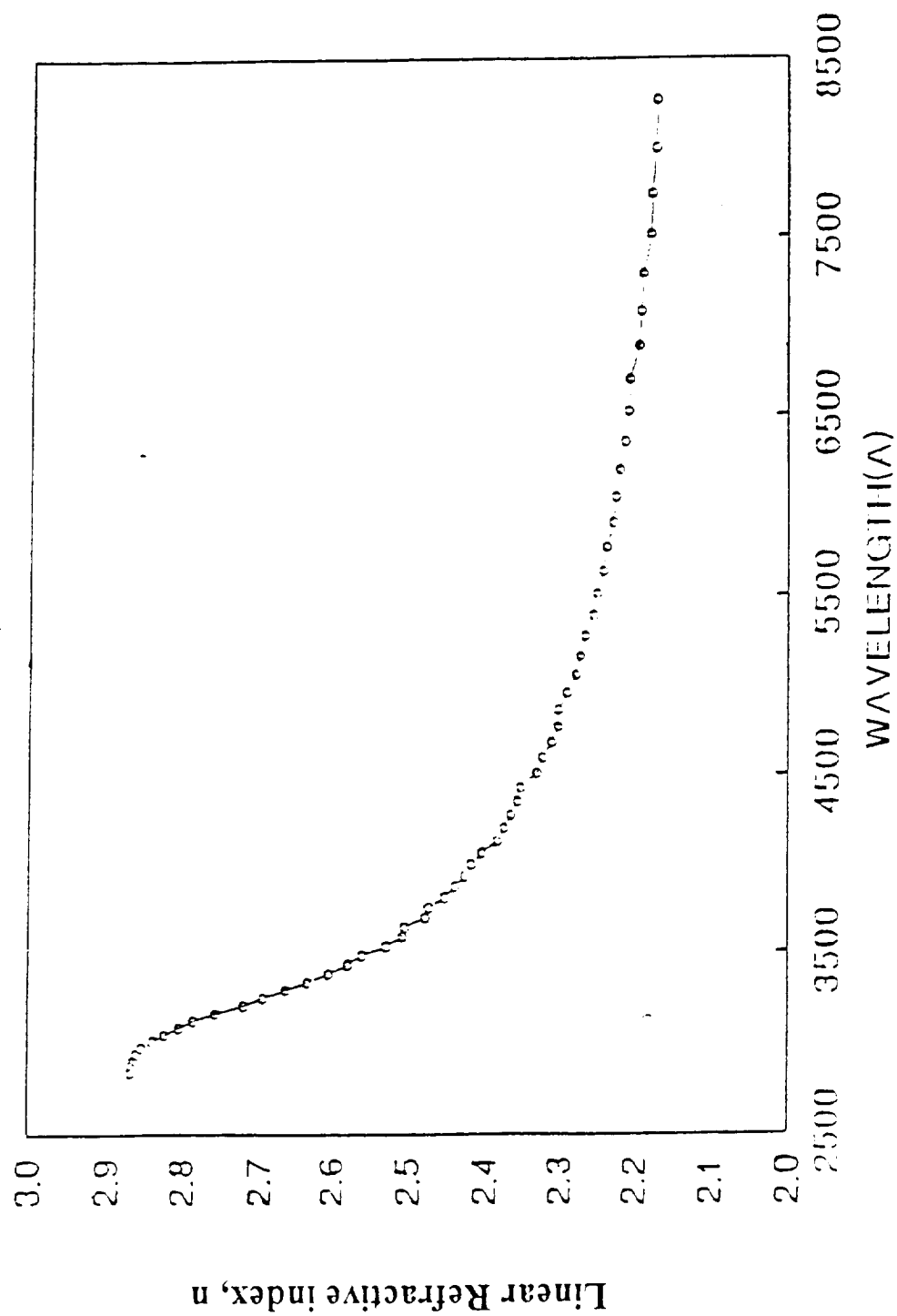
Fig. 30. Linear refractive index, n, as measured by an ellipsometer for a 10PbO-20NbO$_{2.5}$-70TeO$_2$, cat%, (PNT-7) glass as a function of wavelength.